Ki-67 supports global gene expression programmes driving tumourigenesis 2

K Mrouj, P. Singh, M Sobecki, G Dubra, Al Ghoul, A Aznar, Susana Prieto, C Vincent, F Bernex, Benoit Bordignon, et al.

Ki-67 supports global gene expression programmes driving tumourigenesis

Mrouj, K.[1,2,3], Singh, P.[1,2,4], Sobecki, M.[1,2,5], Dubra, G.[1,2], Al Ghoul, E.[1,2], Aznar, A.[1,2], Prieto, S.[1,2], , Vincent, C.[6], Pirot, N.[6,7], Bernex, F. [6,7], Bordignon, B.[8], Hassen-Khodja, C.[8], Pouzolles, M.[1], Zimmerman, V.[1], Dardalhon, V.[1], Villalba, M.[9], Krasinska, L.[1,2] and Fisher, D.[1,2,*]

* Corresponding author

[1]Institut de Génétique Moléculaire de Montpellier (IGMM), University of Montpellier, CNRS, Montpellier, France

[2]Equipe Labellisée LIGUE 2018, Ligue Nationale Contre le Cancer, Paris, France

[3]Present address : Department of Developmental Biology, Stanford University School of Medicine, Stanford, CA 94305, USA

[4]Present address : University of Zurich, Institute of Anatomy, Zurich, Switzerland

[5]Present address : Columbia University Medical Center, New York, USA

[6]Institut de Recherche en Cancérologie de Montpellier (IRCM), Inserm, Montpellier, France

[7]Réseau d'Histologie Expérimentale de Montpellier (RHEM), CNRS, Montpellier, France

[8]Montpellier Ressources en Imagerie (MRI), CNRS, Montpellier, France

[9]Institut de Médecine Régénératrice et Biothérapie (IRMB), Inserm, CHU Montpellier, Montpellier, France

Abstract

Ki-67 is a nuclear protein universally expressed in proliferating vertebrate cells (1), a characteristic that underlies its widespread use as a cancer biomarker. It organises heterochromatin (2,3) and the mitotic chromosome periphery (2,4–6), but it is dispensable for cell proliferation in vivo2. It thus remains unclear whether Ki-67 confers any advantages to cancer cells. Here, using mouse models of breast and intestinal cancer, we show that Ki-67 ensures gene expression programmes required for both carcinogenesis and tumour immunogenicity. We find that germline disruption of Ki-67 protects mice against intestinal tumourigenesis, while in mammary carcinoma cells, ablation of Ki-67 slows tumour growth and inhibits metastasis, despite the failure of cells lacking Ki-67 to induce an effective anti-tumour immune response. Mechanistically, Ki-67 loss leads to widespread deregulation of gene expression, including genes involved in the epithelial-mesenchymal transition (EMT), immune responses and drug metabolism. This results in loss of mesenchymal and stem cell characteristics, downregulation of MHC class I expression and sensitisation to various drug classes. Our results suggest that, by structuring chromatin to allow global transcriptome changes, Ki-67 allows cancer cells to adapt to their environment. This is required for all stages of tumourigenesis and drug resistance, but, by maintaining tumour immunogenicity, it also confers a targetable vulnerability on cancer cells.

Results and discussion

Although Ki-67 is universally expressed in dividing cancer cells, cell proliferation is not affected by Ki-67 gene disruption in any cell type yet analysed *in vitro*, nor during mouse development[2,5–7]. However, Ki-67 might still be important in carcinogenesis since it contributes to organisation of chromatin[2], which controls gene expression and thus cellular plasticity, a characteristic of cancer cells[8,9]. We first tested the involvement of Ki-67 in tumour initiation using an *in vitro* model. We transduced our previously generated *Mki67*$^{+/+}$ or TALEN-mutated *Mki67*$^{-/-}$ 3T3 fibroblasts[10] with oncogenic mutant H-Ras (G12V), and assessed colony formation as an indicator of transformation. While H-Ras^{G12V}-transduced control 3T3 cells efficiently formed colonies, *Mki67*$^{-/-}$ 3T3 cells did not, indicating that Ki-67 expression is required for transformation (Extended Data Fig. 1). We next determined whether Ki-67 knockout affects tumour initiation *in vivo*. We used a mouse model of colon carcinogenesis induced chemically by azoxymethane / dextran sodium sulphate (AOM-DSS) treatment[11], and tested the effect of a germline TALEN-disruption of Ki-67 (*Mki67*$^{2nt\Delta/2nt\Delta}$) that we generated[10]. As expected, AOM-DSS efficiently induced colon tumours within 16 weeks in wild-type and *Mki67*$^{2nt\Delta/+}$ mice; however, no macroscopic lesions were observed in *Mki67*$^{2nt\Delta/2nt\Delta}$ mice

(Fig.1a,b). We confirmed that this was not due to an inability to induce inflammation, since DSS alone triggered similar inflammatory responses in mice of all genotypes (Extended Data Fig. 2). Furthermore, immune cell proliferation and differentiation in *Mki67*$^{2nt\Delta/2nt\Delta}$ mice appeared normal in response to haemolytic anaemia triggered by phenylhydrazine treatment (Extended Data Fig. 3). This suggests that Ki-67 is specifically required for initiation of tumourigenesis. To confirm this, we used a genetic model of intestinal tumourigenesis. We crossed *Mki67*$^{2nt\Delta/2nt\Delta}$ mice with *Apc*$^{\Delta 14/+}$ mice, which rapidly develop tumours in the intestine due to loss of the second allele of the *Apc* tumour suppressor gene[12]. While *Apc*$^{\Delta 14/+}$ *Mki67*$^{2nt\Delta/+}$ mice formed multiple intestinal tumours as expected, tumour burden was strongly reduced in *Apc*$^{\Delta 14/+}$ *Mki67*$^{2nt\Delta/2nt\Delta}$ mice (Fig. 1c,d). These results indicate that Ki-67 is required for efficient initiation of tumourigenesis induced either by an oncogene, chemical mutagenesis or loss of a tumour suppressor.

We next asked whether Ki-67 is required for tumour growth and metastasis from already transformed cells. As a first approach, we knocked down Ki-67 by stable shRNA in a commonly used aggressive human cervical cancer cell line, HeLa S3, and grafted the resulting cells and an shRNA control line into opposing flanks of athymic nude mice. Ki-67 knockdown was maintained *in vivo* (Extended Data Fig. 4a,b) and, as expected, this did not affect cell proliferation (as shown by unchanged PCNA and mitotic indices; Extended data Fig. 4c,d). However, tumour growth was severely slowed (Fig. 2a) and histopathological analysis showed vast areas of necrosis and apoptosis accompanied by disorganised vascular and lymphatic networks, indicating disrupted angiogenesis (Fig. 2b,c). To ensure that phenotypes of Ki-67 downregulation were not specific to the tumour type or knockdown approach, we generated a biallelic *MKI67* gene knockout (KO) by CRISPR-Cas9 in human MDA-MB-231 triple negative breast cancer cells (Extended Data Fig. 4e,f). As expected, *MKI67*$^{-/-}$ cells proliferated normally *in vitro* (Extended Data Fig. 4g,h) but tumours from xenografts in nude mice grew much slower than controls, again showing normal cell proliferation but defective angiogenesis (Fig. 2d-f). Thus, in xenograft experiments, Ki-67 sustains tumour growth but not by controlling cell proliferation.

To determine effects of Ki-67 loss in a mouse model that more closely mimics human breast cancer, we used 4T1 mammary carcinoma cells. This cell line is derived from BALB/c mice, is highly tumourigenic, spontaneously metastasises to distant organs[13,14], and, when grafted in a syngeneic background, a biphasic tumour progression profile is observed due to an induced immune response[15]. As expected, CRISPR-Cas9-mediated *Mki67* knockout did not affect 4T1 cell proliferation rates (Extended Data Fig. 5a-d). We engrafted WT and Ki-67 knockout 4T1 cells orthotopically into mammary fat pads in both immune-proficient syngeneic

BALB/c mice and immunodeficient (athymic-nude and NOD/SCID) mice, the comparison of which should allow identification of the effects of the immune system. In immunodeficient mice, tumours from *Mki67*$^{-/-}$ 4T1 cells grew significantly slower than from Ki-67-expressing 4T1 cells (Fig. 3a-c). In immune-proficient BALB/c mice, control 4T1 tumours established quickly and, as expected, initially regressed before regrowing (Fig. 3d). However, in these mice, *Mki67*$^{-/-}$ 4T1 cells formed primary tumours as efficiently as controls, but no initial regression occurred, overriding the slower growth of knockout tumours and resulting in higher final tumour burden than controls (Fig. 3d). This suggested a defective immune response in mice bearing Ki-67 knockout tumours. We analysed this by immunophenotyping of spleens and lymph nodes. The fraction of dendritic cells, B-cells and T-cells (except for T-reg) was reduced in *Mki67*$^{-/-}$ 4T1 tumour-bearing mice, as a result of a dramatic increase in cells positive for CD11b (a common myeloid marker, expressed by monocytes, neutrophils, NK cells, granulocytes, macrophages and myeloid-derived suppressor cells (MDSC)) (Extended Data Fig. 6). In agreement, immunohistological analysis revealed increased infiltration of MDSC in knockout tumours (using the MDSC marker, GR1; Fig. 3e), possibly indicating an immunosuppressive environment that protects the tumours against immune-mediated cytotoxicity.

In immune-proficient mice, despite the impaired immune-response to *Mki67*$^{-/-}$ 4T1 cells and a consequently higher tumour burden, there were noticeably less metastases than from control 4T1 cells, although this failed to reach statistical significance ($p = 0.13$) (Fig 3f). However, the reduction in visible metastasis from *Mki67*$^{-/-}$ 4T1 cells was highly significant in immunodeficient mice (Fig. 3g) or in immune-proficient mice injected in the tail vein to circumvent the immune-targeting of tumour cells at the primary-site (Fig. 3h). We quantified micrometastases in nude mice by dissociating lung tissue after 2 weeks and growing cells in the presence of 6-thioguanine, to which 4T1 cells are resistant[14]. The number of metastatic cells from Ki-67 knockouts was reduced nearly 100-fold (Extended Data Fig. 7). These results highlight a trade-off for cancer cells, whereby Ki-67 expression sustains tumour growth and promotes metastasis, yet also confers efficient targeting by the immune system.

Since we previously found that Ki-67 knockout in mouse NIH3T3 cells or knockdown in human cancer cells does not alter cell proliferation nor induce cell death, but disrupts chromatin organisation[2] and alters gene expression, we hypothesised that the latter might explain the requirements for Ki-67 in tumourigenesis. To explore this idea we first compared transcriptomes of WT and *Mki67*$^{-/-}$ NIH3T3 cells by RNA-seq. Consistent with roles for Ki-67 in maintaining global chromatin organisation, this revealed widespread changes in gene expression, with 2558 genes significantly deregulated in independent clones of *Mki67*$^{-/-}$ cells

($q < 0.05$) (Extended Data Fig. 8a; Supplementary Table 1). Next, we investigated how transcriptomes are remodelled in 4T1 cells lacking Ki-67. In these cancer cells, *Mki67* knockout caused genome-scale gene expression alterations: 4979 genes were deregulated, of which 1239 and 585 genes were >2-fold down-regulated and up-regulated, respectively (Fig. 4a; Extended Data Fig. 8b; Supplementary Table 2). There was little overlap in the deregulated genes between *Mki67*$^{-/-}$ (epithelial) and NIH3T3 (mesenchymal) cells (Extended Data Fig. 8b; Supplementary Tables 1,2) suggesting that Ki-67 ensures gene expression programmes in different cell types by maintaining chromatin organisation rather than directly regulating specific genes. RNA-seq of early stage tumours from WT and Ki-67 mutant 4T1 cells grafted into nude mice showed that Ki-67-dependent transcriptome changes were preserved *in vivo* (Fig. 4b).

We performed pathway analysis of genes highly deregulated in Ki-67 knockout 4T1 cells to better understand the links between Ki-67-mediated gene expression control and tumourigenesis. We found upregulation of Notch targets and downregulation of genes involved in the inflammatory response, Wnt pathway and the EMT (Fig. 4c) which we validated by qRT-PCR (Extended Data Fig. 8c). Importantly, although the Notch pathway is oncogenic in T cell acute lymphoid leukaemia, it can act as a tumour suppressor in specific cellular contexts[16], can block Wnt signaling[17,18] (a driver of tumourigenesis, cell stemness and the EMT) and induce drug resistance[19]. We confirmed Notch pathway upregulation at the protein level (Fig. 4d). We further verified that Ki-67 knockout 4T1 cells had lost expression of the mesenchymal marker vimentin but upregulated E-cadherin, and had a more epithelial morphology (Fig. 4e). Downregulated genes were enriched in targets of nuclear factor erythroid 2-related factor 2 (NFE2L2), which upregulates genes in response to oxidative stress; interferon regulatory factor 8 (IRF8); polycomb-repression complex 2 (PRC2), which mediates H3K27me3 and is a well-characterised regulator of the EMT[20,21]; and the pluripotency factors Nanog and Sox2 (Extended Data Fig. 8d). We focused on PRC2 as we previously found[10] that in human osteosarcoma U2OS cells, Ki-67 binds to the essential PRC2 component SUZ12. To test whether the repression of the EMT in Ki-67 knockout depends on PRC2, we disrupted *Suz12* or *Ezh2* in WT and *Mki67*$^{-/-}$ 4T1 cells using CRISPR-Cas9. This partially rescued expression of vimentin (Extended Data Fig. 8e,f). However, it did not restore tumour growth rates nor metastasis *in vivo* from *Mki67*$^{-/-}$ 4T1 cells, nor affect tumourigenicity of control cells, in nude mice (Extended Data Fig. 8g). Thus, the PRC2 complex activity is restrained by Ki-67, but does not in itself have either oncogenic or tumour suppressive activity in this system. As such, the reported PRC2 roles in cancer[22,23] might not

apply generally, and a single chromatin regulation pathway cannot account for Ki-67 roles in supporting the EMT and tumourigenesis.

Like Ki-67, the EMT is required for metastasis in some mouse cancer models[24,25]. The EMT is also closely associated with a stem-like state[26–28], as well as resistance to chemotherapeutic drugs[29] and induction of immune responses[30]. We therefore next investigated the importance of Ki-67 for these three EMT-linked characteristics.

First, we analysed two indicators of tumour cell stemness: the ability to form spheroids in the absence of adhesion to a surface[26,31], and aldehyde dehydrogenase activity[32,33]. Both parameters were strongly reduced in Ki-67 knockout 4T1 cells (Fig. 4f,g).

Second, we noticed that 26 genes involved in drug metabolism were downregulated in Ki-67 knockout 4T1 cells, while only one was upregulated, suggesting that Ki-67 expression might determine sensitivity to chemotherapeutic drugs (Extended Data Fig. 9a,b). To test this, we performed an automated gene-drug screen using the Prestwick chemical library, composed of 1283 FDA-approved small molecules, as well as salinomycin, a positive control found to target cancer stem cells[34], and 6-thioguanine, which was originally used to isolate 4T1 cells[13]. Control 4T1 cells were sensitive to 102 drugs at 10μM concentration, while the two *Mki67*$^{-/-}$ clones were sensitive to 99 and 98 respectively, with 82 hits common to the three cell lines (Extended Data Fig. 9c; Supplementary Data). This suggests that Ki-67 loss does not qualitatively alter the drug-sensitivity profiles. We next determined the IC_{50} of 10 common hits used in cancer therapy. Importantly, *Mki67*$^{-/-}$ cells were markedly more sensitive to all the molecules tested (Fig. 4h; Extended Data Fig. 9d).

Third, genes directing mouse major histocompatibility complex (MHC) class I-mediated antigen presentation *Tap2, Psmb8* and *Psmb9* were downregulated in *Mki67*$^{-/-}$ 4T1 cells (Extended Data Fig. 8c; Supplementary Table 2). Flow cytometry confirmed lower expression of the mouse MHC class I molecules H2D and H2K (Fig. 4i), providing an explanation for how Ki-67 knockout affects tumour recognition by the immune system. We obtained similar results in human *MKI67*$^{-/-}$ MDA-MB-231 cells, implying that roles of Ki-67 in maintaining MHC expression are conserved across species (Extended Data Fig. 10).

The above results show that Ki-67 is not required for cancer cell proliferation *in vivo,* but supports coherent transcriptional programmes that are involved in tumour cell plasticity, drug resistance and induction of immune responses. Together, these likely account for the roles of Ki-67 in tumourigenesis revealed in this study (Fig. 4j). Clues to its biochemical mechanism of action are suggested by the fact that Ki-67 is an intrinsically disordered protein (IDP) and behaves as a surfactant for mitotic chromatin[5]. Since we previously found that heterochromatin is more dispersed in cells lacking Ki-67 (ref. 2), we propose that these

properties may also allow Ki-67 to regulate interphase chromatin. Due to their conformational flexibility, IDPs can act as hubs to bind many protein partners[35], and we previously identified many chromatin regulators interacting with Ki-67 (ref. 2). However, disrupting one such interactor, the PRC2 complex, does not restore tumourigenic capacity to Ki-67 mutant cancer cells, consistent with the idea that Ki-67 may act more globally.

While it has long been thought that global changes in nuclear structure observed in cancer cells might contribute functionally to carcinogenesis[36], mechanistic insight into this question has been lacking. We speculate that the alterations of nuclear organisation seen in cancer cells may reflect their increased cellular plasticity. By binding multiple chromatin regulators and organising the transcriptome at a genome scale, Ki-67 might contribute to both nuclear structuration and cellular plasticity, thereby conferring on cancer cells the ability to adapt to their environment.

References

1. Endl, E. & Gerdes, J. The Ki-67 protein: fascinating forms and an unknown function. *Exp Cell Res* **257**, 231–7 (2000).
2. Sobecki, M. *et al.* The cell proliferation antigen Ki-67 organises heterochromatin. *eLife* **5**, e13722 (2016).
3. Sun, X. *et al.* Ki-67 Contributes to Normal Cell Cycle Progression and Inactive X Heterochromatin in p21 Checkpoint-Proficient Human Cells. *Mol. Cell. Biol.* **37**, (2017).
4. Booth, D. G. *et al.* Ki-67 is a PP1-interacting protein that organises the mitotic chromosome periphery. *eLife* **3**, e01641 (2014).
5. Cuylen, S. *et al.* Ki-67 acts as a biological surfactant to disperse mitotic chromosomes. *Nature* **535**, 308–312 (2016).
6. Takagi, M., Natsume, T., Kanemaki, M. T. & Imamoto, N. Perichromosomal protein Ki67 supports mitotic chromosome architecture. *Genes Cells* **21**, 1113–1124 (2016).
7. Cidado, J. *et al.* Ki-67 is required for maintenance of cancer stem cells but not cell proliferation. *Oncotarget* **7**, 6281–6293 (2016).
8. Ben-Porath, I. *et al.* An embryonic stem cell-like gene expression signature in poorly differentiated aggressive human tumors. *Nat. Genet.* **40**, 499–507 (2008).
9. Kim, J. *et al.* A Myc network accounts for similarities between embryonic stem and cancer cell transcription programs. *Cell* **143**, 313–324 (2010).
10. Sobecki, M. *et al.* The cell proliferation antigen Ki-67 organises heterochromatin. *eLife* **5**, (2016).

11. De Robertis, M. *et al.* The AOM/DSS murine model for the study of colon carcinogenesis: From pathways to diagnosis and therapy studies. *J. Carcinog.* **10**, 9 (2011).
12. Colnot, S. *et al.* Colorectal cancers in a new mouse model of familial adenomatous polyposis: influence of genetic and environmental modifiers. *Lab. Investig. J. Tech. Methods Pathol.* **84**, 1619–30 (2004).
13. Dexter, D. L. *et al.* Heterogeneity of tumor cells from a single mouse mammary tumor. *Cancer Res.* **38**, 3174–3181 (1978).
14. H Heppner, G., R Miller, F. & Malathy Shekhar, P. Nontransgenic models of breast cancer. *Breast Cancer Res.* **2**, (2000).
15. Tao, K., Fang, M., Alroy, J. & Sahagian, G. G. Imagable 4T1 model for the study of late stage breast cancer. *BMC Cancer* **8**, 228 (2008).
16. Nowell, C. S. & Radtke, F. Notch as a tumour suppressor. *Nat. Rev. Cancer* **17**, 145–159 (2017).
17. Nicolas, M. *et al.* Notch1 functions as a tumor suppressor in mouse skin. *Nat. Genet.* **33**, 416–421 (2003).
18. Devgan, V. p21WAF1/Cip1 is a negative transcriptional regulator of Wnt4 expression downstream of Notch1 activation. *Genes Dev.* **19**, 1485–1495 (2005).
19. Meng, R. D. *et al.* -Secretase Inhibitors Abrogate Oxaliplatin-Induced Activation of the Notch-1 Signaling Pathway in Colon Cancer Cells Resulting in Enhanced Chemosensitivity. *Cancer Res.* **69**, 573–582 (2009).
20. Malouf, G. G. *et al.* Architecture of epigenetic reprogramming following Twist1-mediated epithelial-mesenchymal transition. *Genome Biol.* **14**, R144 (2013).
21. Tiwari, N. *et al.* Sox4 is a master regulator of epithelial-mesenchymal transition by controlling Ezh2 expression and epigenetic reprogramming. *Cancer Cell* **23**, 768–783 (2013).
22. Chase, A. & Cross, N. C. P. Aberrations of EZH2 in Cancer. *Clin. Cancer Res.* **17**, 2613–2618 (2011).
23. Bracken, A. P. & Helin, K. Polycomb group proteins: navigators of lineage pathways led astray in cancer. *Nat. Rev. Cancer* **9**, 773–784 (2009).
24. Ye, X. *et al.* Upholding a role for EMT in breast cancer metastasis. *Nature* **547**, E1–E3 (2017).
25. Aiello, N. M. *et al.* Upholding a role for EMT in pancreatic cancer metastasis. *Nature* **547**, E7–E8 (2017).

26. Mani, S. A. *et al.* The epithelial-mesenchymal transition generates cells with properties of stem cells. *Cell* **133**, 704–715 (2008).
27. Morel, A.-P. *et al.* Generation of breast cancer stem cells through epithelial-mesenchymal transition. *PloS One* **3**, e2888 (2008).
28. Wellner, U. *et al.* The EMT-activator ZEB1 promotes tumorigenicity by repressing stemness-inhibiting microRNAs. *Nat. Cell Biol.* **11**, 1487–1495 (2009).
29. Zheng, X. *et al.* Epithelial-to-mesenchymal transition is dispensable for metastasis but induces chemoresistance in pancreatic cancer. *Nature* **527**, 525–530 (2015).
30. López-Soto, A. *et al.* Epithelial-mesenchymal transition induces an antitumor immune response mediated by NKG2D receptor. *J. Immunol. Baltim. Md 1950* **190**, 4408–4419 (2013).
31. Ishiguro, T. *et al.* Tumor-derived spheroids: Relevance to cancer stem cells and clinical applications. *Cancer Sci.* **108**, 283–289 (2017).
32. Ginestier, C. *et al.* ALDH1 Is a Marker of Normal and Malignant Human Mammary Stem Cells and a Predictor of Poor Clinical Outcome. *Cell Stem Cell* **1**, 555–567 (2007).
33. Huang, E. H. *et al.* Aldehyde Dehydrogenase 1 Is a Marker for Normal and Malignant Human Colonic Stem Cells (SC) and Tracks SC Overpopulation during Colon Tumorigenesis. *Cancer Res.* **69**, 3382–3389 (2009).
34. Gupta, P. B. *et al.* Identification of selective inhibitors of cancer stem cells by high-throughput screening. *Cell* **138**, 645–659 (2009).
35. Wright, P. E. & Dyson, H. J. Intrinsically disordered proteins in cellular signalling and regulation. *Nat. Rev. Mol. Cell Biol.* **16**, 18–29 (2015).
36. Zink, D., Fischer, A. H. & Nickerson, J. A. Nuclear structure in cancer cells. *Nat. Rev. Cancer* **4**, 677–687 (2004).

Acknowledgements

We thank D. Grimanelli for help with transcriptome analysis, and P. Jay, D. Santamaria, M.E. Hochberg and M. Serrano for comments on the manuscript. K.M and M.S. were funded by the Ligue Nationale Contre le Cancer (LNCC); P.S. and K.M. received funding from Worldwide Cancer Research (WWCR). D.F. and L.K. are Inserm employees. This work was initiated and finalised with support from the LNCC and continued with support from Worldwide Cancer Research (WWCR) and the French National Cancer Institute (INCa). The chemical library screen relied on support provided by the Programme Opérationnel FEDER-FSE 2014-2020 Languedoc Roussillon.

Competing interests

The authors declare that they have no competing interests.

Author Contributions

D.F. conceived and supervised the project. K.M., L.K., V.Z., M.V. and D.F. designed experiments and interpreted the data. K.M., M.S., P.S., E.A., A.A., S.P., C.V., N.P., F.B., B.B., M.P., C.H-K. and V.D. performed experiments. G.D. performed data analysis. K.M., L.K. and D.F. wrote the manuscript.

Data availability

All RNA-seq raw data will be deposited in GEO and will be publicly available prior to publication of the manuscript.

Fig.1

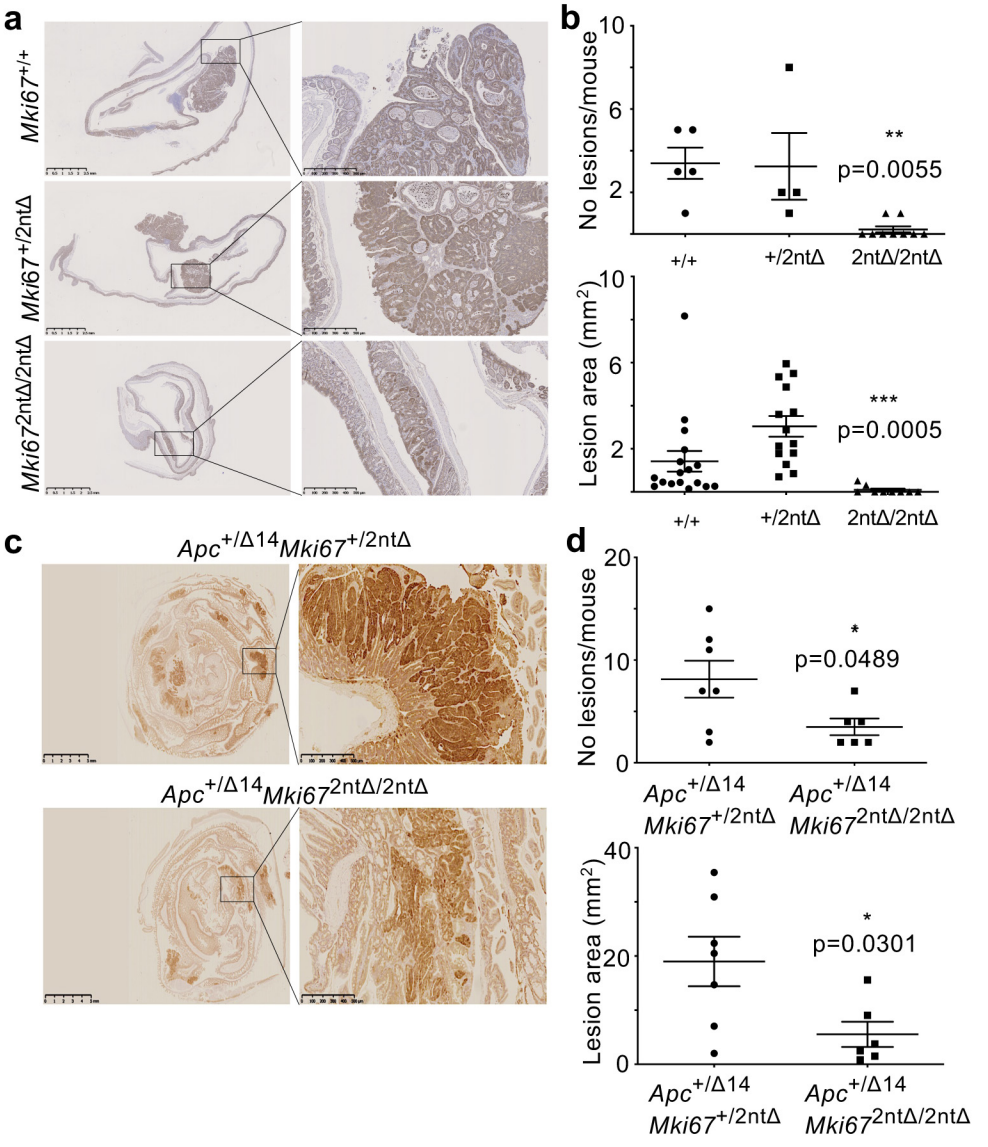

Figure 1: **Germline disruption of Ki-67 protects mice against intestinal tumourigenesis.**
a. IHC analysis of β-catenin expression in whole intestines recovered from each mouse group (*Mki67*$^{+/+}$; *Mki67*$^{+/2ntΔ}$ and *Mki67*$^{2ntΔ/2ntΔ}$) at week-16 post AOM-DSS treatment. Scale bar, 2.5mm. Insets show accumulation of β-catenin in nuclei. Scale bar, 500μm. **b**. Quantification of the number (top) and area (bottom) of neoplastic lesions. Error bar, SEM (n= 5 *Mki67*$^{+/+}$ mice; n= 4 *Mki67*$^{+/2ntΔ}$ mice; n= 9 *Mki67*$^{2ntΔ/2ntΔ}$ mice). **c**. IHC staining of β-catenin in whole intestines from 6-7-month old *Apc*$^{+/Δ14}$*Mki67*$^{+/2ntΔ}$ and Apc$^{+/Δ14}$*Mki67*$^{2ntΔ/2ntΔ}$ mice. Scale bar, 5mm. Insets show accumulation of β-catenin in nuclei. Scale bar, 500μm. **d**. Quantification of the number (top) and total area (bottom) of neoplastic lesions. Error bars, SEM (n= 7 *Apc*$^{+/Δ14}$*Mki67*$^{+/2ntΔ}$ mice; n= 6 Apc$^{+/Δ14}$*Mki67*$^{2ntΔ/2ntΔ}$ mice).

Fig.2

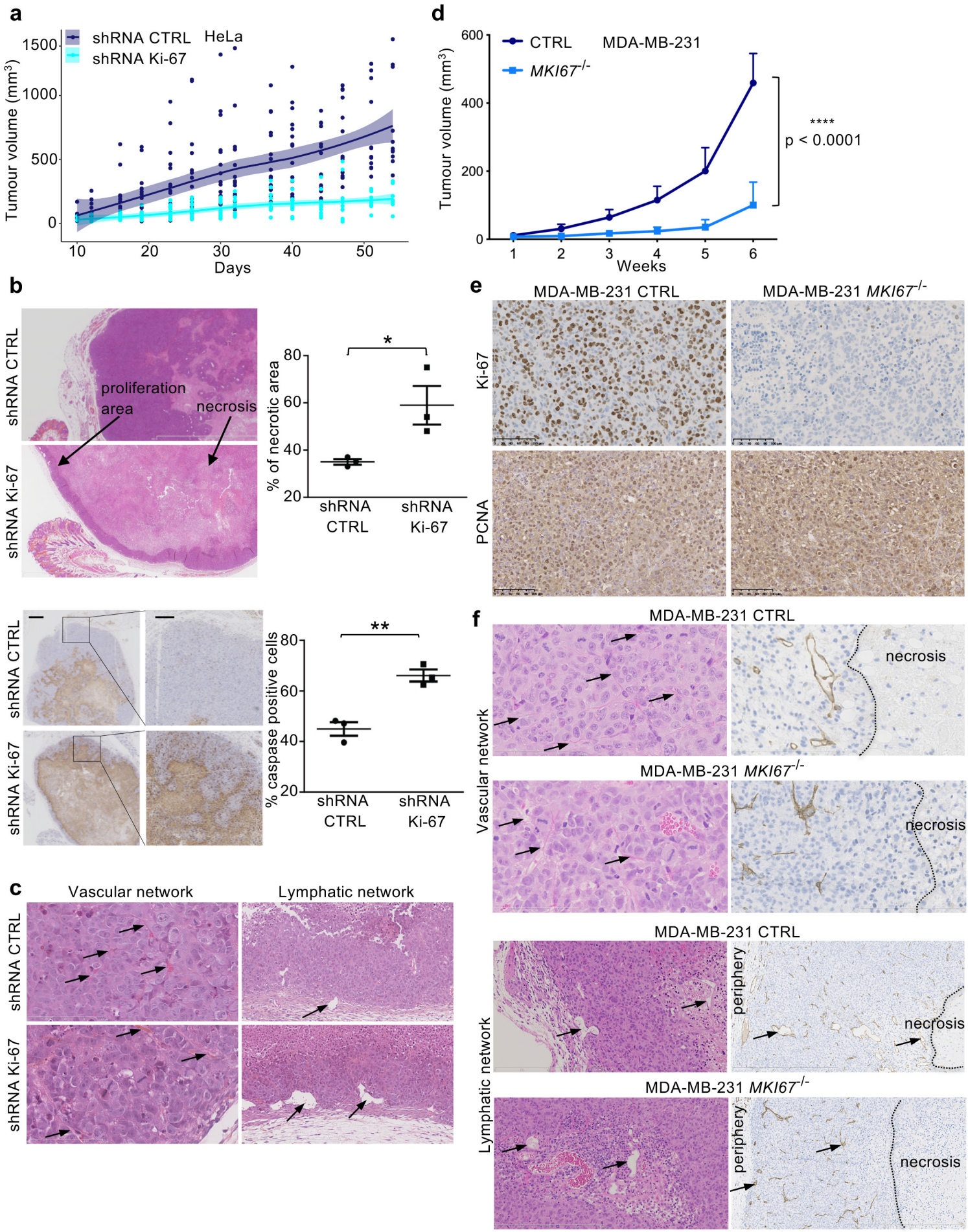
a
shRNA CTRL HeLa
shRNA Ki-67
Tumour volume (mm3)
Days
d
CTRL MDA-MB-231
MKI67-/-
Tumour volume (mm3)
Weeks
****
p < 0.0001
b
shRNA CTRL
shRNA Ki-67
proliferation area
necrosis
% of necrotic area
shRNA CTRL
shRNA Ki-67
**
% caspase positive cells
e
MDA-MB-231 CTRL
MDA-MB-231 MKI67-/-
Ki-67
PCNA
c
Vascular network
Lymphatic network
f
MDA-MB-231 CTRL
MDA-MB-231 MKI67-/-
Vascular network
Lymphatic network
necrosis
periphery

Figure 2: Ki-67 sustains tumour growth independently of cell proliferation.
a-c. HeLa shRNA CTRL or shRNA Ki-67 were injected subcutaneously into 6-8-week old nude mice. **a**. Tumour burden (n=19 mice). **b**. (Top left) Hematoxylin and eosin (H&E)-stained tumour sections highlighting proliferation and necrotic areas. Scale bar, 3mm. (Top right) Percentage of necrotic area for each of 3 separate tumours from different mice per cell line, mean ± SEM. (Bottom left) Immunohistochemistry (IHC) staining for cleaved caspase 3. Scale bar, 1mm (250μm for insets). (Bottom right) Percentage of cleaved caspase 3-positive cells for tumours from different mice, mean ± SEM. **c**. H&E-stained tumour sections showing vascular (arrows; scale bar, 100μm) and lymphatic networks (arrows; scale bar, 400μm). While in CTRL tumours fibrovascular network is thin and regular, in shRNA Ki-67 tumours, the network is disorganised, thick and fibrosed. The lymph vessels in shRNA Ki-67 tumours are dilated, characteristic for oedema and indicative of slow fluid flow. **d-f**. Xenografts of MDA-MB-231 CTRL or Ki-67 KO cells in mammary fat pads of nude mice. **d**. Tumour burden. Error bars, SEM (n=8 mice). **e**. IHC images of tumours stained for Ki-67 and PCNA. Scale bar, 100μm. **f**. IHC analysis of vascular and lymphatic networks (arrows). Left, H&E; scale bar, 400μm. Right, CD31 staining; scale bar, 800μm. Areas of necrosis are indicated. The defects in Ki-67 KO tumours are similar as those observed in shRNA Ki-67 tumours.

Fig. 3

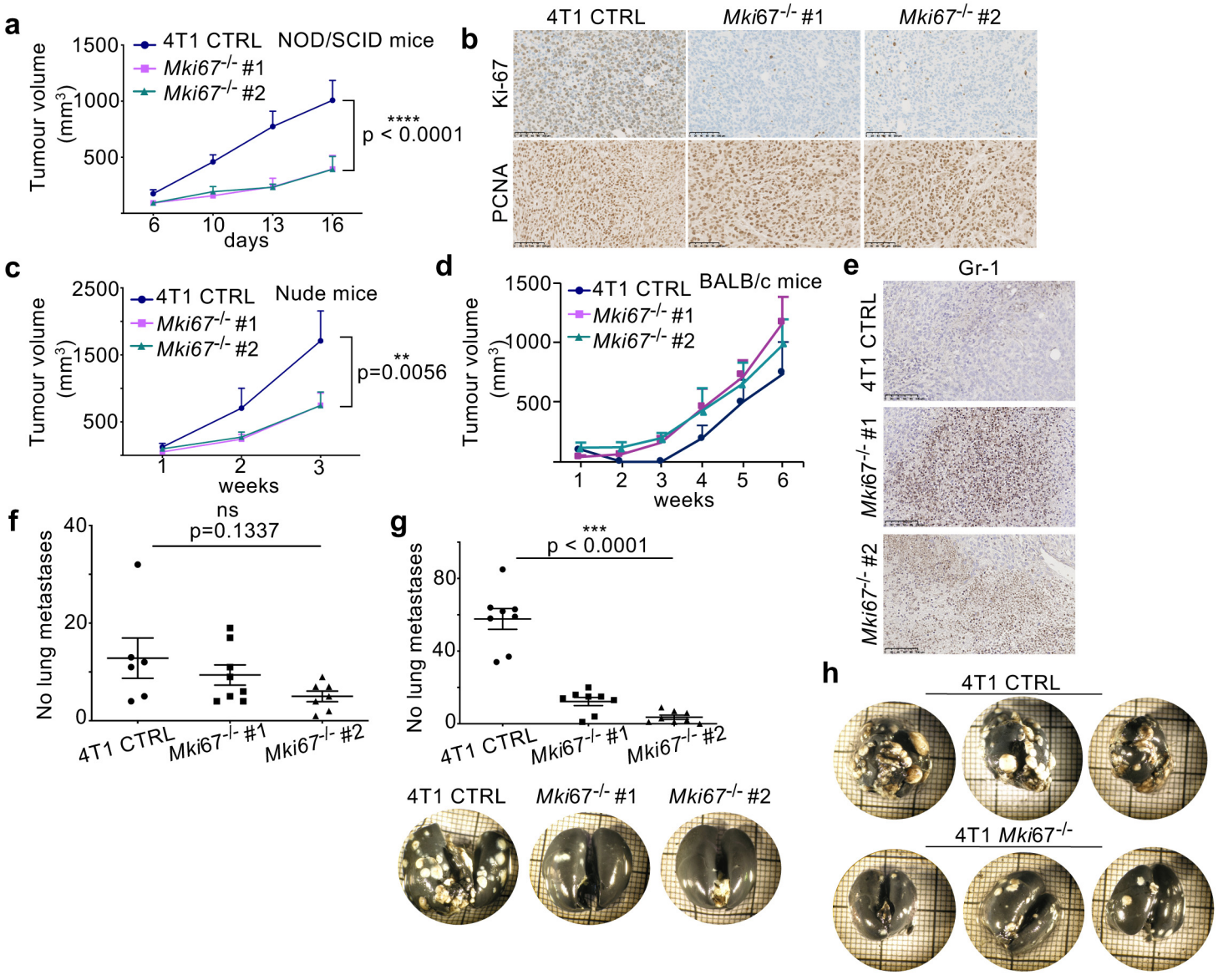

Figure 3: Metastasis and anti-tumour immune responses require Ki-67.
a. 4T1 CTRL or *Mki67*$^{-/-}$ orthotopic xenografts in NOD/SCID mice. Tumour growth was monitored for 3 weeks (left). Error bars, SEM (n=6 mice). **b**. IHC staining for Ki-67 and PCNA in 4T1 CTRL or *Mki67*$^{-/-}$ tumours. Scale bar, 100μm. **c**. 4T1 CTRL or *Mki67*$^{-/-}$ orthotopic xenografts in athymic nude mice. Error bars, SEM (n=8 mice). **d**. Tumour growth of 4T1 CTRL or *Mki67*$^{-/-}$ orthotopic xenografts in immunocompetent BALB/c mice. Error bars, SEM (n=8 mice). **e**. IHC analysis of 4T1 CTRL or *Mki67*$^{-/-}$ tumours (week-4 post-transplantation) stained for Gr-1, a myeloid-derived suppressor cell (MDSC) marker. Scale bar, 100μm. **f**. Quantification of lung metastases in BALB/c mice in **d**. Error bars, SEM. **g**. Quantification of lung metastases in nude mice in **c**. Error bars, SEM. Bottom, representative images of lungs stained to visualise metastases (white nodules); scale bar, 10mm. **h**. 4T1 CTRL or *Mki67*$^{-/-}$ cells were injected via tail vein into immune-competent BALB/c mice. Representative images of stained lungs (day 21 post-injection), metastases are white. Scale bar, 10mm.

Fig. 4

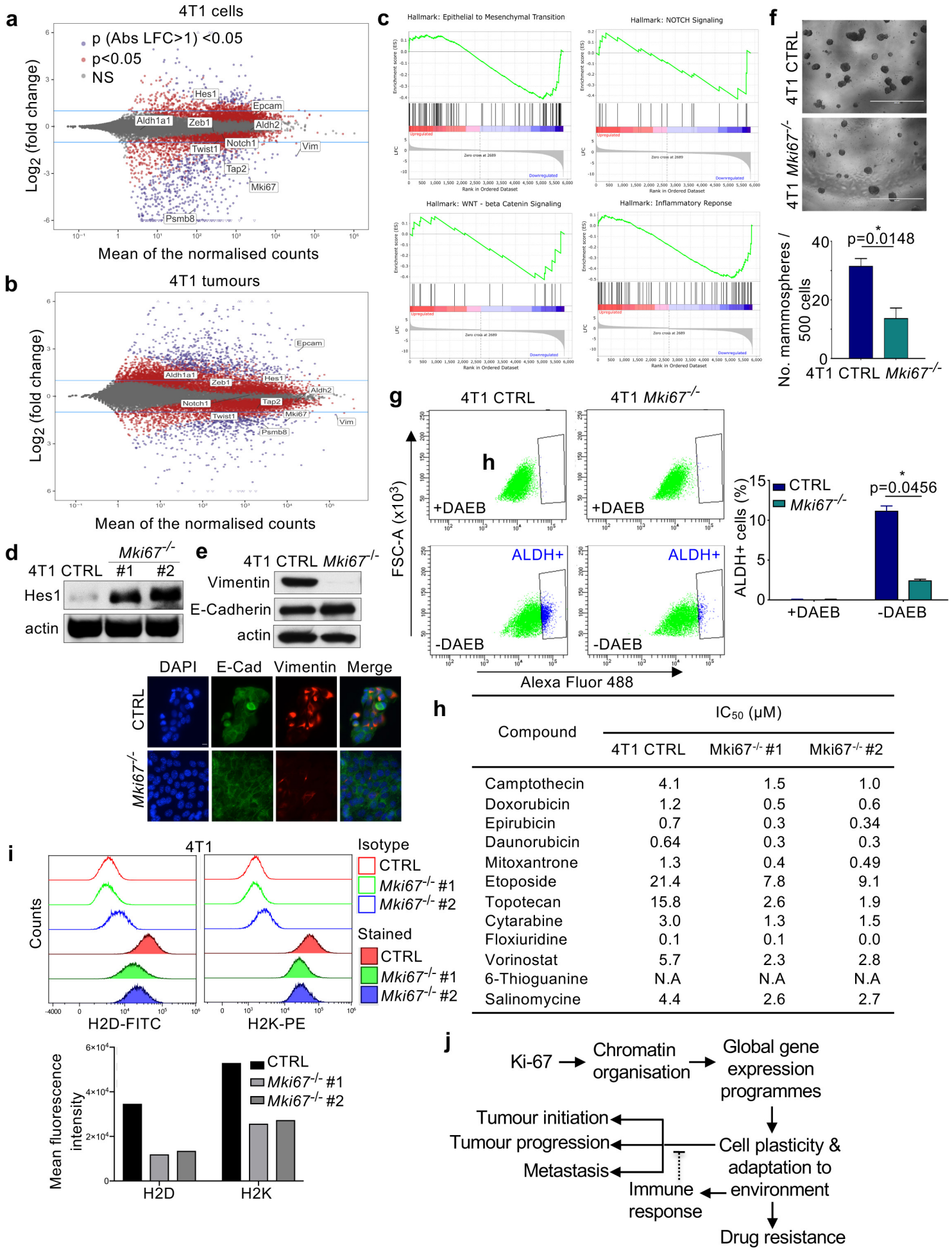

h

Compound	IC50 (μM)		
	4T1 CTRL	Mki67-/- #1	Mki67-/- #2
Camptothecin	4.1	1.5	1.0
Doxorubicin	1.2	0.5	0.6
Epirubicin	0.7	0.3	0.34
Daunorubicin	0.64	0.3	0.3
Mitoxantrone	1.3	0.4	0.49
Etoposide	21.4	7.8	9.1
Topotecan	15.8	2.6	1.9
Cytarabine	3.0	1.3	1.5
Floxiuridine	0.1	0.1	0.0
Vorinostat	5.7	2.3	2.8
6-Thioguanine	N.A	N.A	N.A
Salinomycine	4.4	2.6	2.7

Figure 4: **Ki-67 ablation deregulates gene expression programmes involved in cancer cell stemness, drug resistance and immunogenicity**.
a,b. Dot plot analysis of differentially expressed genes (DEGs) in 4T1 *Mki67*$^{-/-}$ cells (**a**) and 4T1 *Mki67*$^{-/-}$-derived tumours (**b**). Red dots: DEGs with adjusted p-value < 0.05; purple dots: genes whose $\log_2$ fold change, LFC >1 or <-1, is statistically significant (adjusted p-value < 0.05); grey dots: not significant, NS. **c**. Gene Set Enrichment Analysis (GSEA) of highly down-regulated genes in 4T1 *Mki67*$^{-/-}$ cells. **d**. Immunoblot analysis of Hes1 expression in 4T1 CTRL and *Mki67*$^{-/-}$ cells. **e**. Immunoblot (top) and immunofluorescence (bottom; scale bar, 10µm) analysis of vimentin and E-cadherin expression in 4T1 CTRL and *Mki67*$^{-/-}$ cells. **f**. Mammosphere formation assay of 4T1 CTRL or *Mki67*$^{-/-}$ cells. Representative images (top; scale bar, 400 µm) and quantification (bottom; error bars, SEM, n=10) after 7 days. **g**. Aldehyde dehydrogenase 1 activity measured using a flow-cytometry assay in 4T1 CTRL and *Mki67*$^{-/-}$ cells. DAEB, inhibitor of ALDH was used as a negative control. Left, representative FACS images. Right, quantification of ALDH+ cells. Error bars, SEM (n=2 independent analyses). **h**. IC_{50} of 4T1 CTRL or *Mki67*$^{-/-}$ cells treated with indicated compounds. **i**. Flow-cytometry analysis of MHC class I expression. 4T1 CTRL and *Mki67*$^{-/-}$ cells were stained with anti-H2D^{d}-FITC and anti-H2K^{d}-PE, or control isotypes. Top, representative images. Bottom, quantification (n=1 of each clone). **j**. Model of Ki-67 mechanism in tumour progression and cancer cell dissemination (see text).

Ext. Fig.1

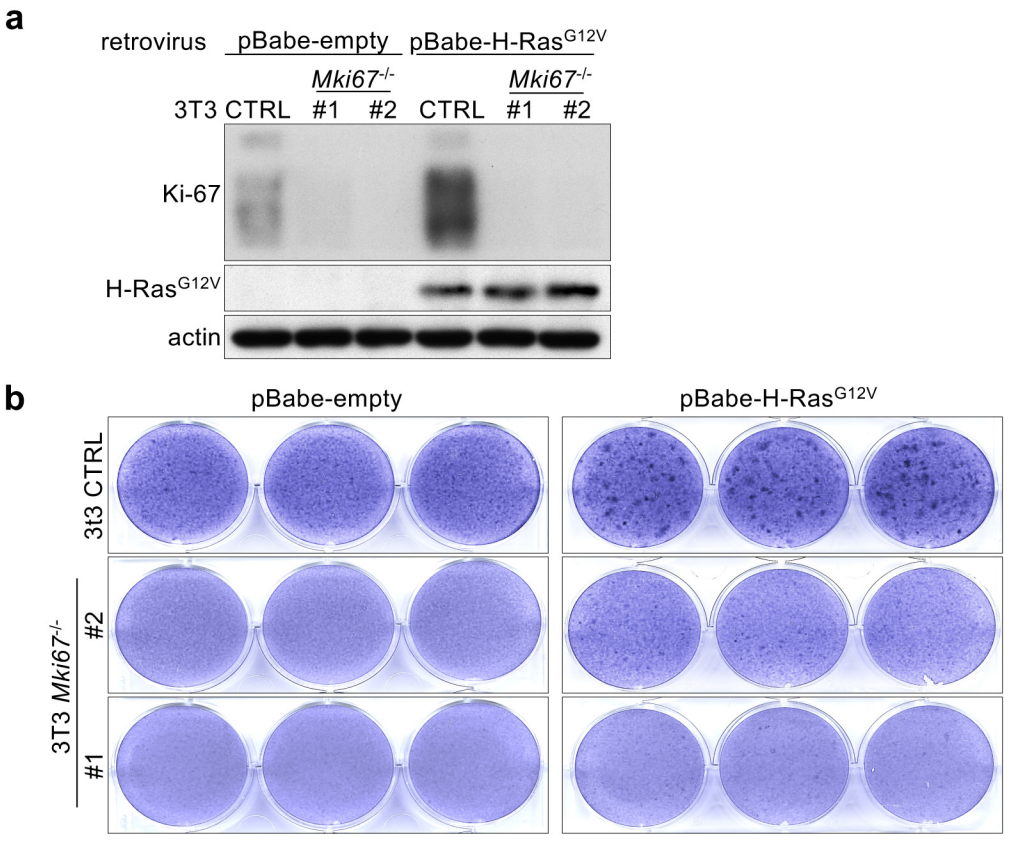

Extended Data Fig. 1: Ki-67 is required for cell transformation.
CTRL or TALEN-mutated *Mki67*$^{-/-}$ 3T3 fibroblasts were transduced with either empty or H-Ras^{G12V}-expressing retroviruses. **a**. Immunoblot analysis of the expression of the indicated proteins. Actin serves as loading control. **b**. Crystal violet staining of the colonies formed.

Ext. Fig.2

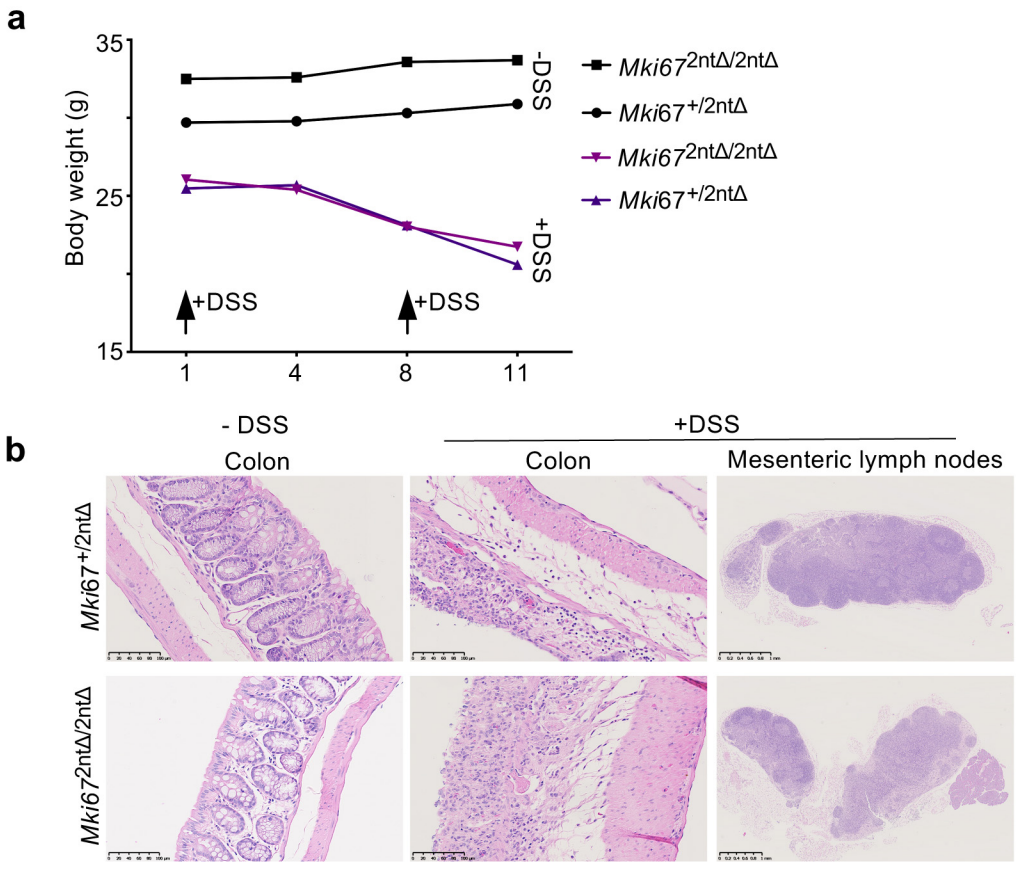

Extended Data Fig. 2: *Mki67*$^{mt/mt}$ mice have normal inflammatory response.
a. Body weight (g) measurement in *Mki67*$^{+/2ntΔ}$ and *Mki67*$^{2ntΔ/2ntΔ}$ mice during the AOM-DSS experiment. **b**. Assessment of inflammatory response in colon and mesenteric lymph nodes in *Mki67*$^{+/2ntΔ}$ and *Mki67*$^{2ntΔ/2ntΔ}$ mice, treated or not with DSS (H&E staining; scale bar, 1mm).

Ext. Fig.3

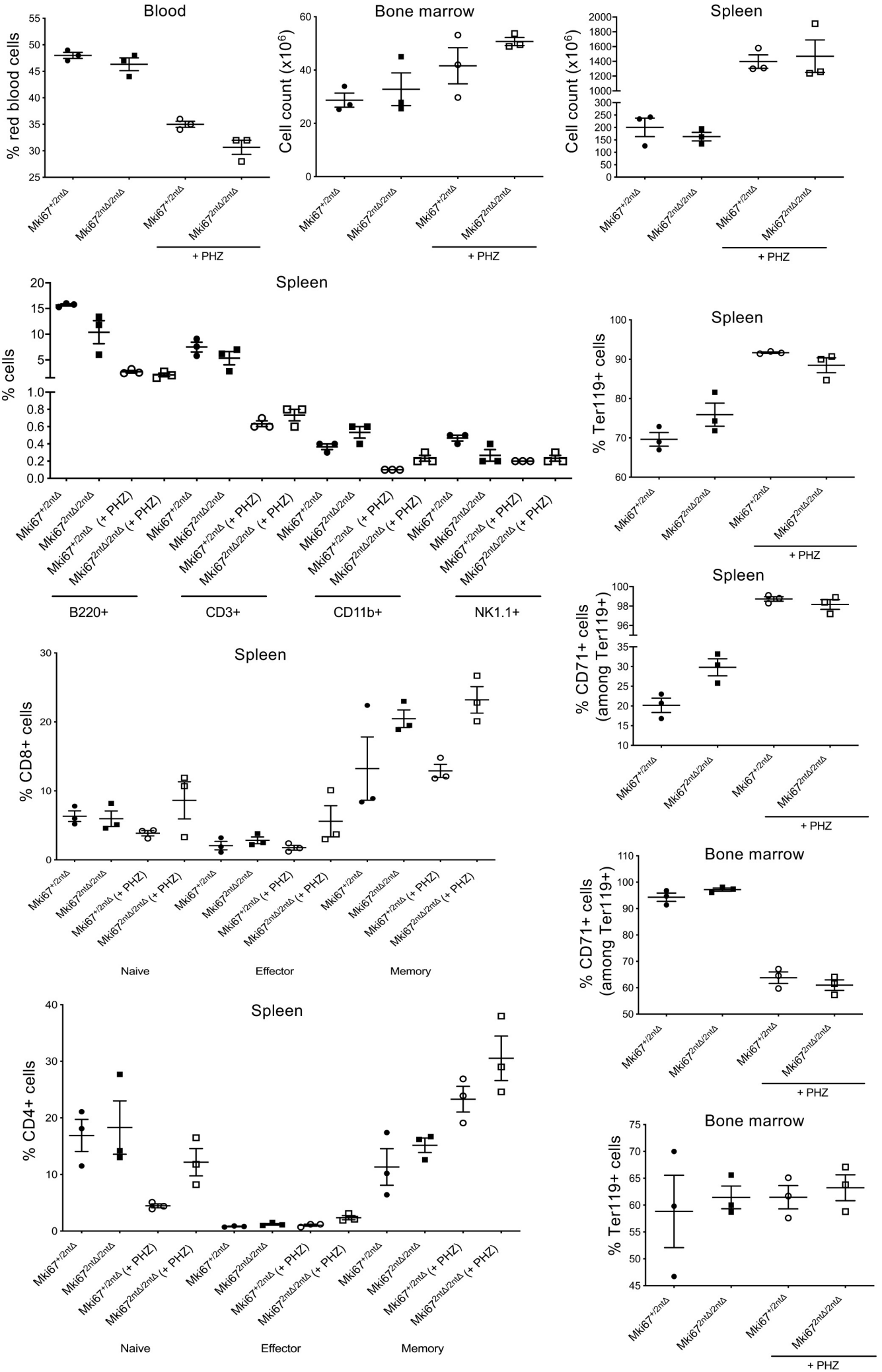

Extended Data Fig. 3: *Mki67*$^{2nt\Delta/2nt\Delta}$ mice have normal response to haemolytic anaemia triggered by phenylhydrazine (PHZ) treatment.

Analysis of number and percentage of indicated populations of blood, bone marrow and spleen cells in *Mki67*$^{+/2nt\Delta}$ and *Mki67*$^{2nt\Delta/2nt\Delta}$ mouse, treated or not with PHZ.

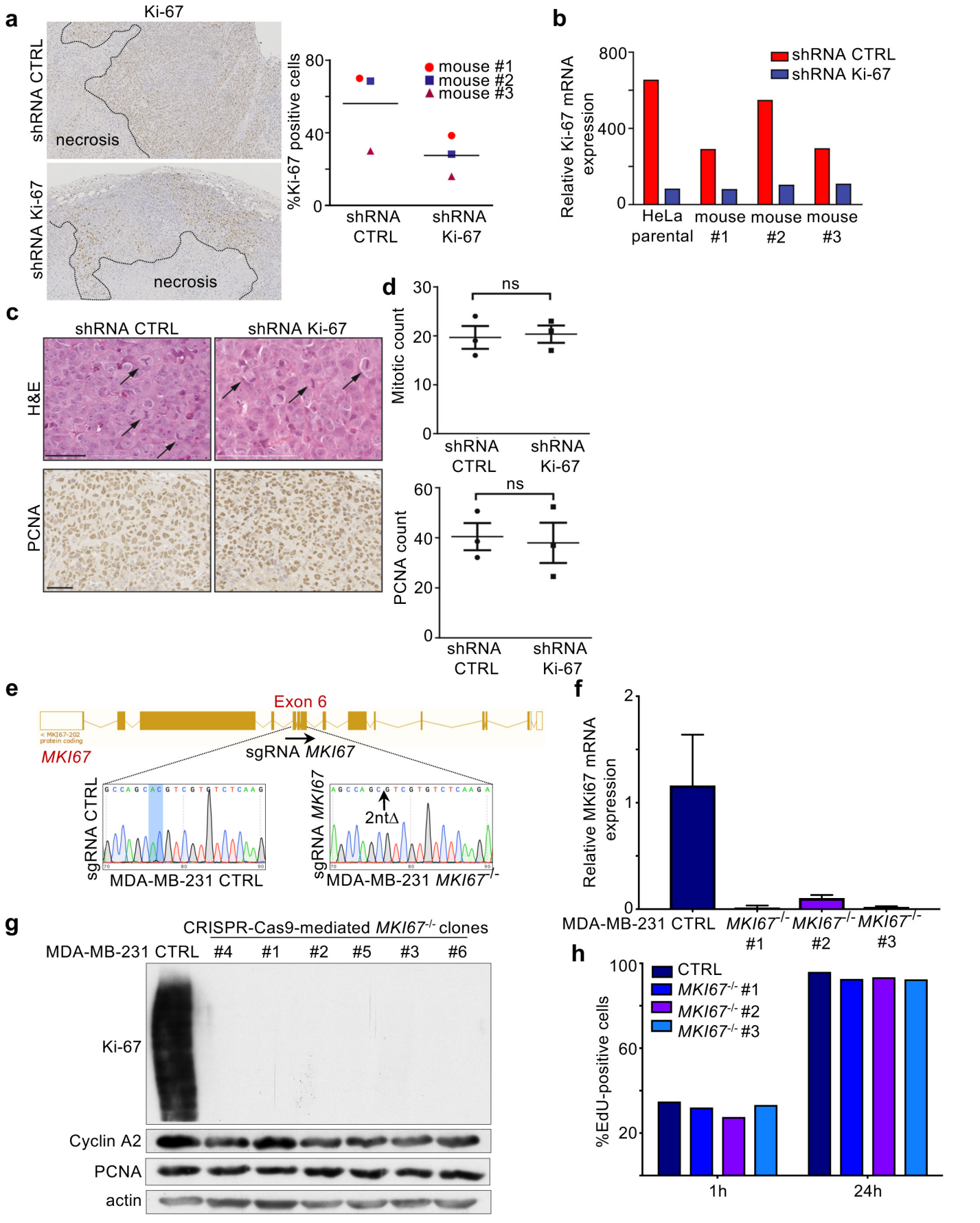

Extended Data Fig. 4: Ablation of Ki-67 does not affect cell proliferation.
a-d. Characterisation of HeLa shRNA CTRL and shRNA Ki-67 xenografts. **a**. Left, IHC staining for Ki-67; necrotic areas are highlighted. Right, quantification of Ki-67-positive cells in tumours (n=3 mice). **b**. Relative Ki-67 mRNA expression levels in HeLa shRNA CTRL and shRNA Ki-67 parental cells and xenografts. **c**. H&E (top; arrows indicate mitotic cells) and PCNA (bottom) staining of HeLa shRNA CTRL and shRNA Ki-67 xenografts. **d**. Quantification of mitotic indices and PCNA-positive cells. **e-h**. Characterisation of MDA-MB-231 CTRL and *MKI67*$^{-/-}$ cells. **e**. Scheme of CRISPR-Cas9-mediated disruption of *MKI67* gene (targeting exon 6 and resulting in a 2nt-deletion). **f**. Relative Ki-67 mRNA expression in parental MDA-MB-231 cells and three *MKI67*$^{-/-}$ clones. **g**. Immunoblotting for the indicated proteins of parental MDA-MB-231 cells and six *MKI67*$^{-/-}$ clones. **h**. Quantification of the number of CTRL and *MKI67*$^{-/-}$ MDA-MB-231 EdU-positive cells, pulsed with EdU for either 1h or 24h.

Ext. Fig.5

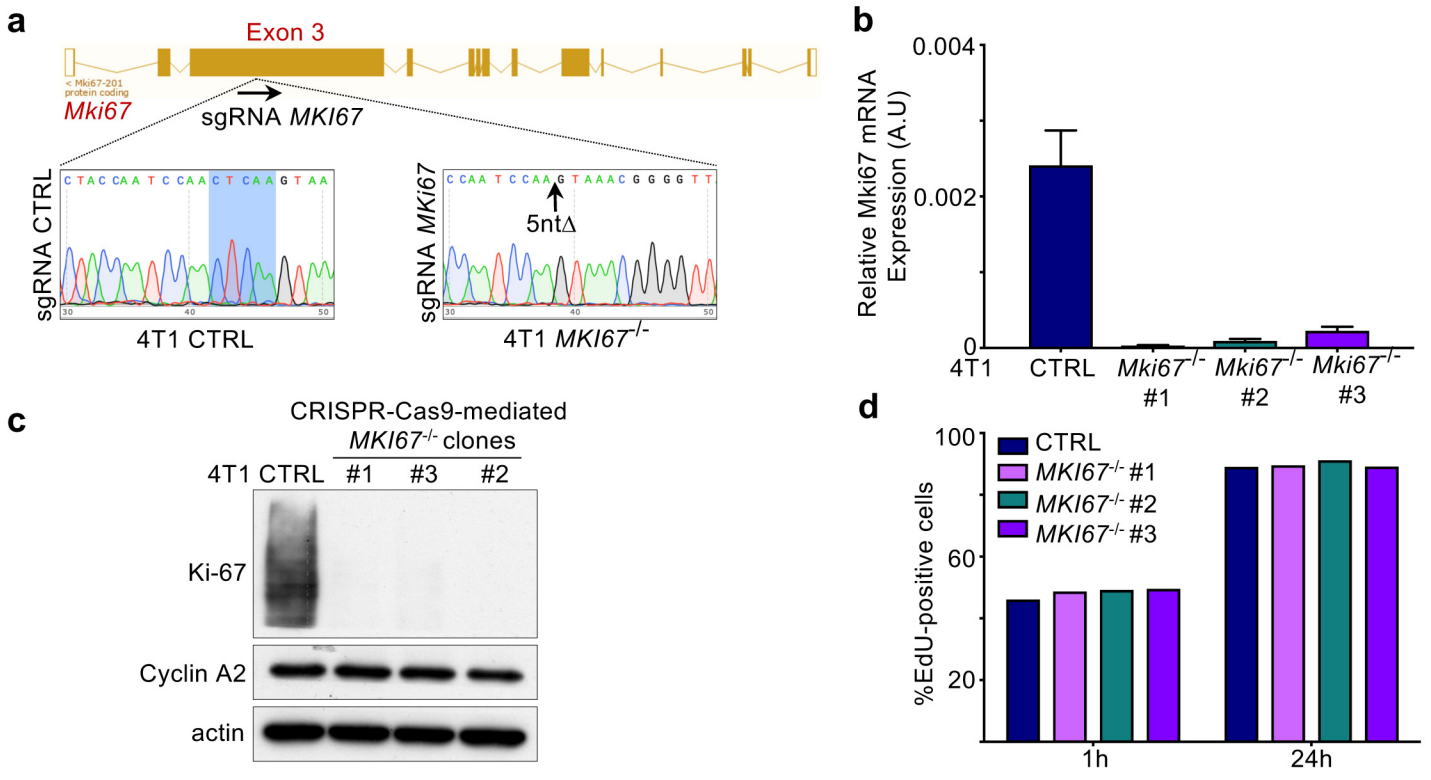

Extended Data Fig. 5: Knockout of *Mki67* in 4T1 cells.
a. Scheme of CRISPR-Cas9-mediated disruption of *Mki67* gene in 4T1 cells (targeting exon 3 and resulting in a 5nt-deletion). **b**. Relative Ki-67 mRNA expression in parental 4T1 cells and three *Mki67*$^{-/-}$ clones. **c**. Immunoblotting for the indicated proteins of parental 4T1 cells and *Mki67*$^{-/-}$ clones. **d**. Quantification of the number of CTRL and *Mki67*$^{-/-}$ EdU-positive cells, pulsed with EdU for either 1h or 24h.

Ext. Fig.6

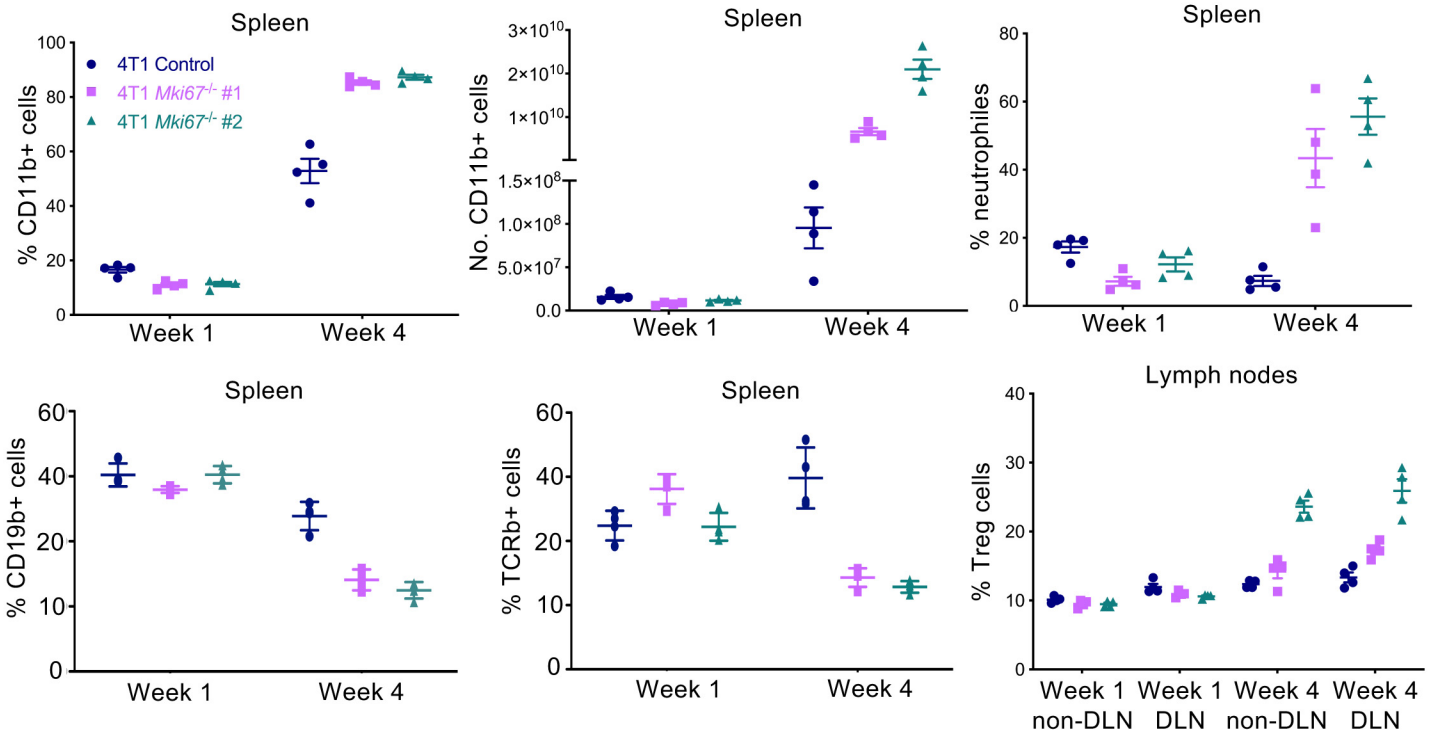

Extended Data Fig. 6: Ki-67 knockout induces an immunosuppressive tumour environment.
Immunohistological analysis of spleens and lymph nodes (draining, DLN; and non-draining, non-DLN) performed in week 1 and 4 in mice xenografted with 4T1 CTRL and *Mki67*$^{-/-}$ cells (n=4).

Ext. Fig.7

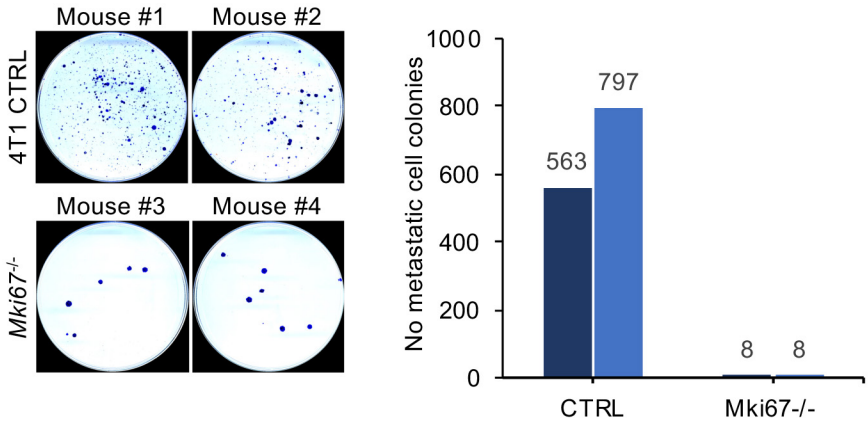

Extended Data Fig. 7: Ki-67 knockout reduces metastatic potential.
Lung tissue from mice injected via tail vein with 4T1 CTRL or *Mki67*$^{-/-}$ cells (2 per condition) was dissociated and resulting cells were maintained in the presence of 6-thioguanine, to select for 4T1 cells. Left, cristal violet staining of resulting colonies. Right, quantification of the number of 4T1 CTRL and *Mki67*$^{-/-}$ colonies.

Ext. Fig.8

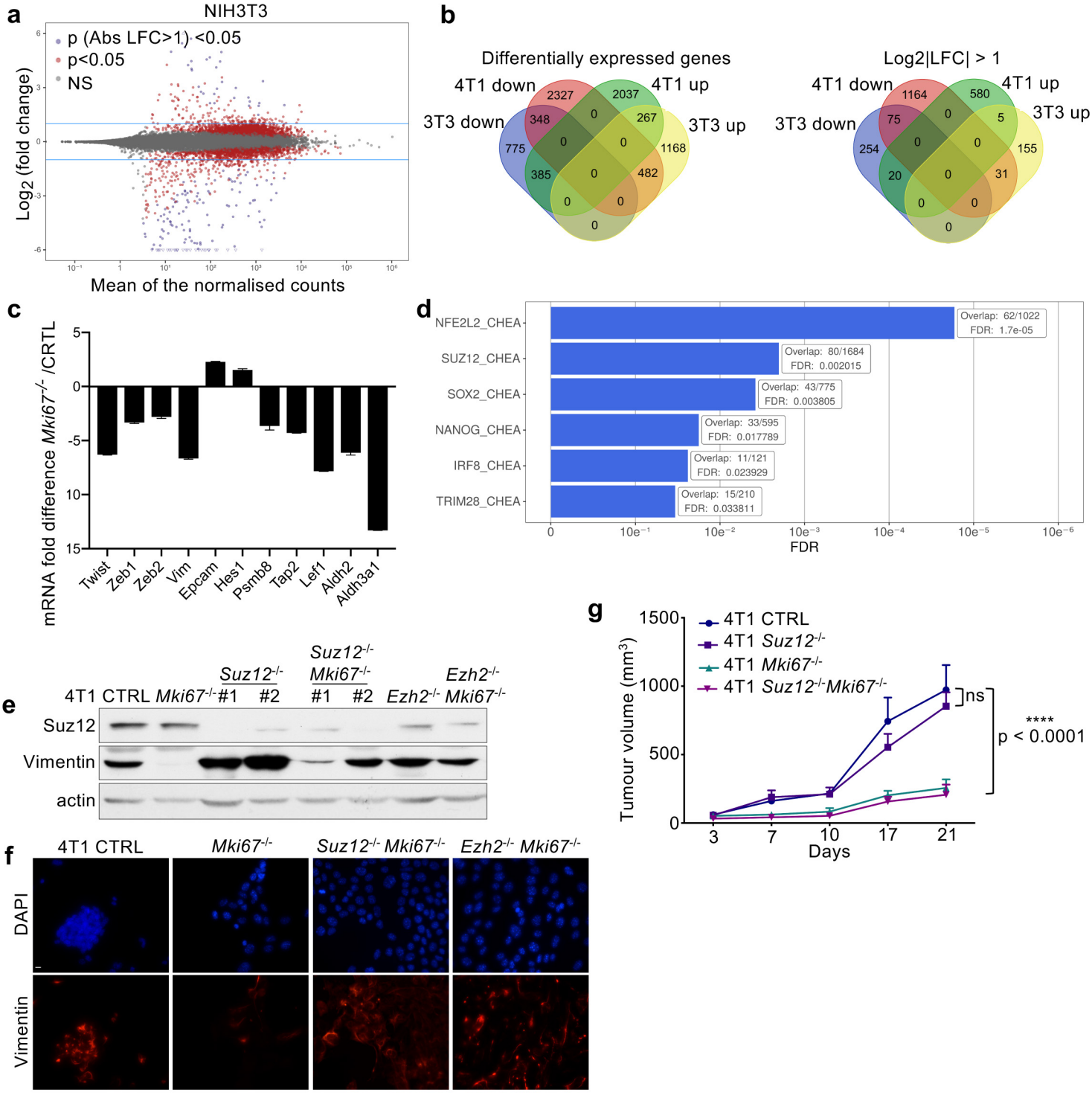

Extended Data Fig. 8: Ki-67 controls gene expression, in part through PRC2.
a. Dot plot analysis of differentially expressed genes (DEGs) in 3T3 *Mki67*$^{-/-}$ cells. Red dots: DEGs with adjusted p-value < 0.05; purple dots: genes whose $\log_2$ fold change, LFC >1 or <-1, is statistically significant (adjusted p-value < 0.05); grey dots: not significant, NS. **b.** Venn diagrams of DEGs in 3T3 and 4T1 *Mki67*$^{-/-}$ cells under condition of p-value < 0.05 (left), and p-value (LFC >1 or <-1) < 0.05 (right). **c.** Quantitative RT-PCR analysis of differentially expressed mesenchymal and epithelial markers in 4T1 *Mki67*$^{-/-}$ cells; fold change in expression ± SD is shown. **d.** Gene set enrichment performed over the ENCODE and ChEA Consensus transcription factors from ChIP-X gene sets. FDR, false discovery rate adjusted p-values. **e.** Western-blot analysis of Suz12 and Vimentin levels in 4T1 cells, CRTL, and single or double knockouts for *Mki67*, *Suz12* and *Ezh2*. Actin serves as loading control. **f.** Immunoflorescence staining of Vimentin in 4T1 CRTL, *Mki67*$^{-/-}$, *Mki67*$^{-/-}$;*Suz12*$^{-/-}$ and *Mki67*$^{-/-}$;*Ezh2*$^{-/-}$ cells. **g.** Tumour growth of 4T1 CTRL, *Suz12*$^{-/-}$, *Mki67*$^{-/-}$, and *Mki67*$^{-/-}$*Suz12*$^{-/-}$ xenografts over 3 weeks (n=3).

Ext. Fig.9

a

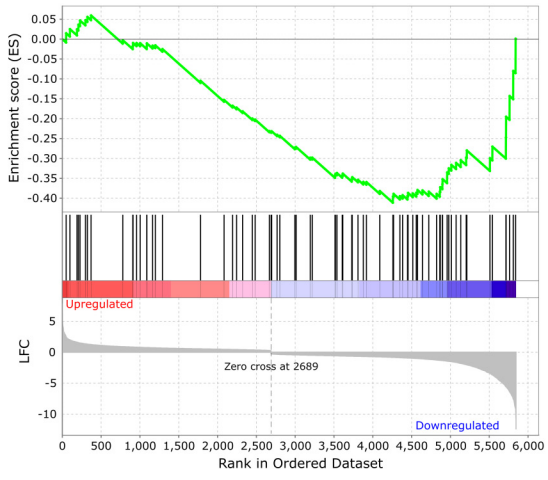

b

Upregulated	Downregulated
Phase I drug metabolising enzymes	
PTGS1	ALDH1l2, 3a1, 1b1 CYP1b1, 2c55, 3a13 PTGS2
Phase II drug metabolising enzymes	
	AOX1 BLVRB EPHX1 GSTA1, 2, 3 GSTM1, 2, 5 GSTT2, 3 MAOA MGST1, 2 NAT2, 6, 9 NQO1 PON3

c

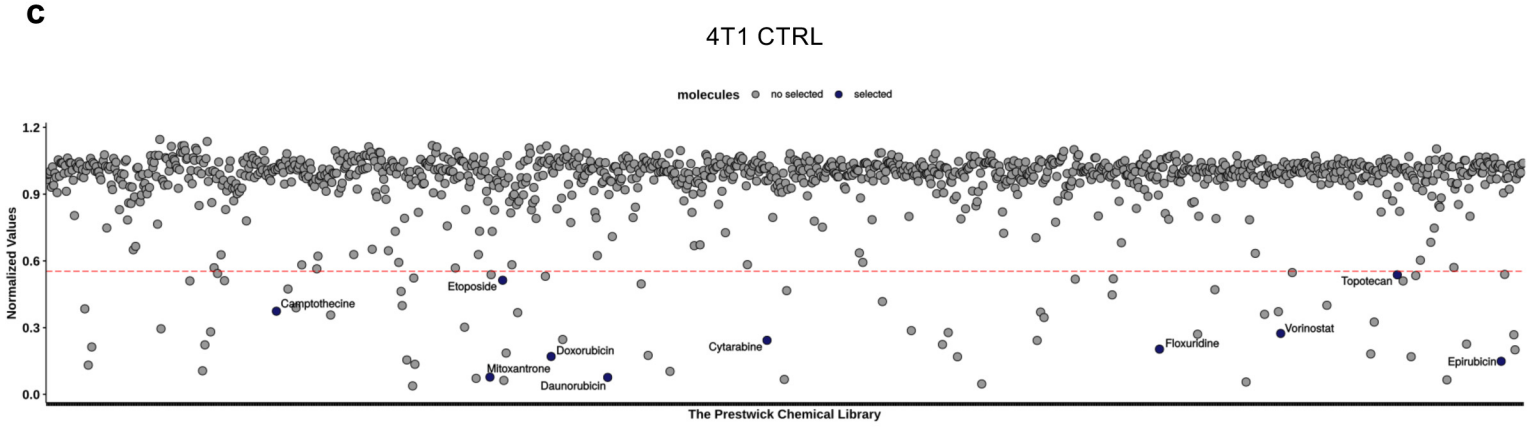

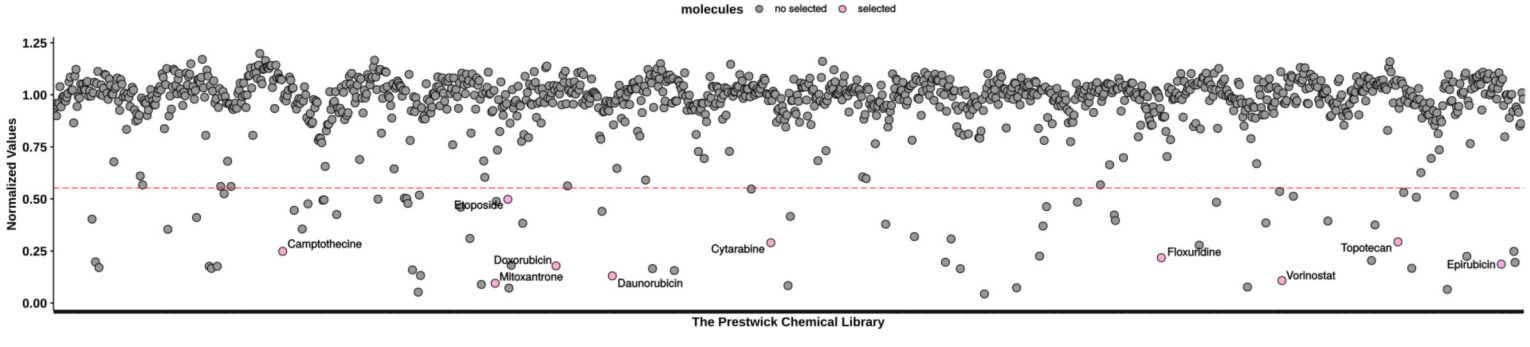

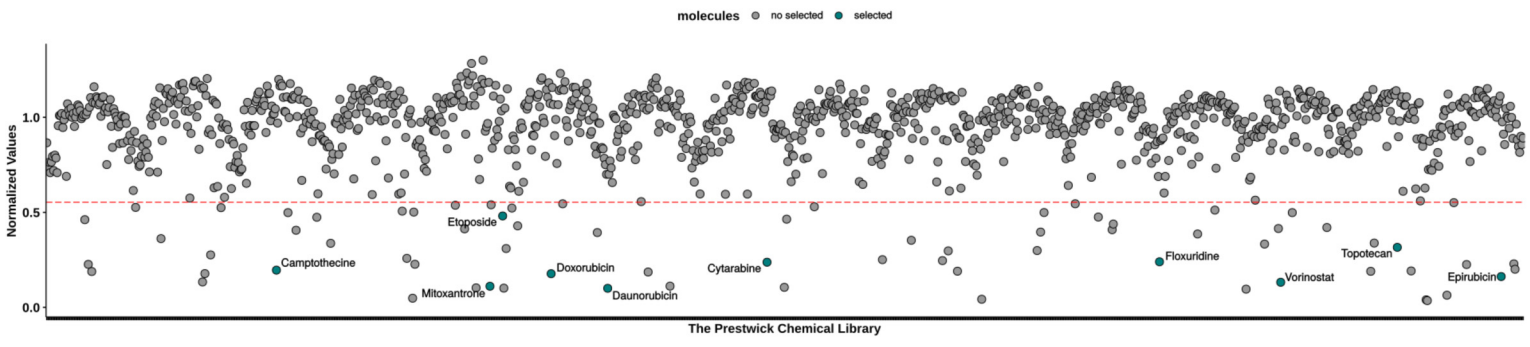

d

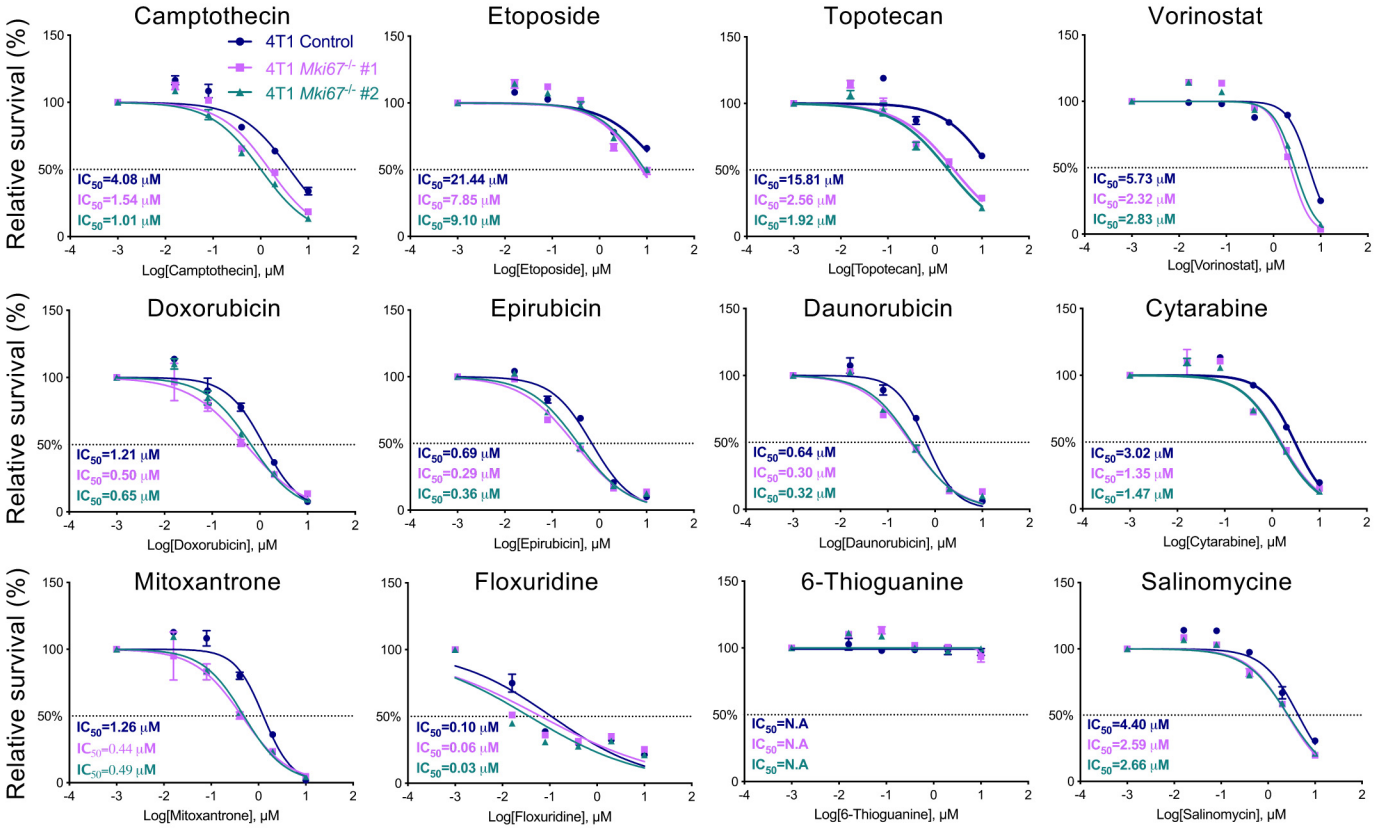

Extended Data Fig. 9: Ki-67 knockout sensitises cells to various drugs.
a. Xenobiotic metabolism is one of hallmarks found in pathway analysis of genes downregulated in *Mki67*$^{-/-}$ cells. **b**. List of drug-metabolising enzymes with altered expression in *Mki67*$^{-/-}$ cells. **c**. Results of the automated gene-drug screen using the Prestwick chemical library. 'Hits' were identified applying the Z-score statistical method and are located below the dashed red line. Drugs chosen for subsequent dose-response experiments are highlighted in colour for CTRL and *Mki67*$^{-/-}$ clones. **d**. Dose-response curves of 4T1 CTRL or *Mki67*$^{-/-}$ cells treated with indicated compounds and their corresponding IC_{50}.

Ext. Fig.10

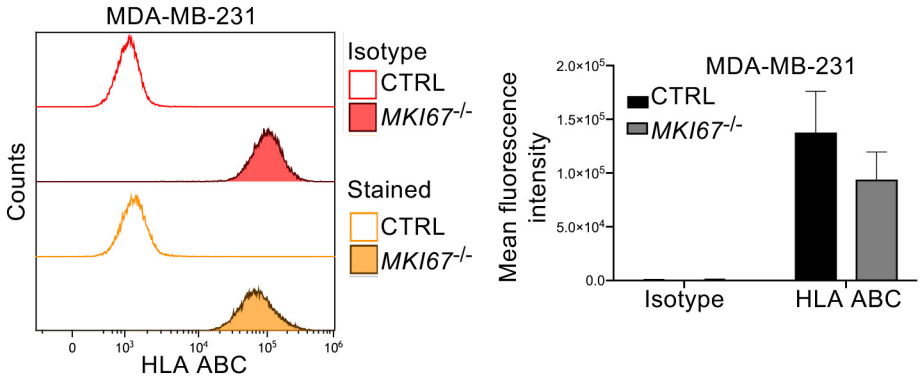

Extended Data Fig. 10. **MHC class I expression requires Ki-67 in MDA-MB-231 cells.** MDA-MB-231 CTRL and *MKI67*$^{-/-}$ cells were stained with anti-HLA-PE or control isotype. Top, representative images of FACS analysis. Bottom, quantification; median ± SD (n=2 independent experiments).

Methods

Cell lines and mice

4T1 cells were provided by Robert Hipskind (IGMM, Montpellier); MDA-MB-231 cells were obtained from SIRIC, Montpellier. NIH 3T3, 4T1, MDA-MB-231 and S3 HeLa cells were grown in Dulbecco modified Eagle medium (DMEM - high glucose, pyruvate, GlutaMAX – Gibco® Life LifeTechnologies) supplemented with 10% foetal bovine serum (SIGMA or DUTSCHER). Cells were grown under standard conditions at 37°C in humidified incubator containing 5% CO_2.

6-8 weeks-old female BALB/c (BALB/cOlaHsd), athymic nude (Hsd:Athymic Foxn1^{nu}/Foxn1^{+}), and NOD.SCID (NOD.CB17-Prkdc^{scid}/NCrHsd) mice were purchased from Envigo. C57BL/6 Apc$^{\Delta 14}$ mice[12] were provided by Philippe Jay (IGF, Montpellier).

Animal studies

All animal experiments were performed in accordance with international ethics standards and were subjected to approval by the Animal Experimentation Ethics Committee of Languedoc Roussillon (n°APAFIS#8637-2017012311188975v3).

Antibodies and plasmids

Antibodies: Ki-67 (clone SP6; Abcam), cyclin A2 (6E6; Novocastra), PCNA (ab18197; Abcam), β-catenin (BD610154; BD-Bioscience), Ras (G12V Mutant Specific D2H12, #14412; CST), actin (A2066; Sigma), vimentin (D21H3, #5741; CST), E-Cadherin (24E10, #3195; CST), Suz12 (D39F6, #3737; CST), H3K27me3 (#39155, Active Motif), H2D^{d}-FITC (#553579; BD Biosciences), H2K^{d}-PE (SF1-1.1; BD Biosciences), HLA-PE (EMR8-5; BD Biosciences).

Lentiviral Vectors used: LentiCRISPRv2 (Addgene #52961), pMD2.G (Addgene #12259), psPAX2 (Addgene #12260). pHIV-Luc-ZsGreen (Addgene #39196) was used to generate bicistronic lentivirus that expresses both Luciferase and Zsgreen.

Retroviral vectors used: pBabe-puro (Addgene #1764), pBabe-puro H-Ras^{G12V} (Addgene #1768). gag/pol (retroviral packaging) and Maloney (envelope) were gift from Leatitia Linares (IRCM, Montpellier).

pUC57-U6-sgRNA (#51132, Addgene); Cas9-VP12 (#72247, Addgene), modified by adding T2A-GFP at the C-terminal end (gift from Edouard Bertrand, IGMM).

CRISPR/Cas9-mediated genome editing

The sgRNAs targeting mouse *Mki67* exon 3 or human *MKI67* exon 6 and non-targeting control sequences were previously designed[37], and cloning of the target sequence into the LentiCRISPRV2 lentiviral vector was conducted as described[37]. Lentiviruses encoding the sgRNA targeting sequences were produced. Transduced cells (4T1 and MDA-MB-231) expressing CRISPR/Cas9 were selected using puromycin. Resistant cells were isolated and seeded as single cell clones in 96 well-plates.

For Suz12 and Ezh2 knockout, sgRNA targeting sequences[37] were synthesised with BpiI sticky ends and cloned into the pUC57-U6-sgRNA vector. Cas9-VP12-T2A-GFP and sgRNA vectors were transfected into 4T1 WT and Ki-67$^{-/-}$ #2 clone using Lipofectamine 2000 (ThermoFisher). 24h post-transfection, GFP-positive cells were sorted i96-well plates by flow cytometry (FACS Aria, BD). After 10-12 days of culture, colonies were picked and screened (Cellomics, Thermo), using Suz12 or H3K9me3 antibodies. Positive knockout clones were confirmed by PCR, IF and western blotting.

AOM-DSS-induced colon carcinogenesis

Mice (*Mki67*$^{+/+}$; *Mki67*$^{+/2nt\Delta}$ & *Mki67*$^{2nt\Delta/2nt\Delta}$) were given a single intraperitoneal injection of AOM (10 mg/kg in 0.9% saline; A5486, Sigma-Aldrich), and one week later, 2% Dextran Sodium Sulfate (DSS; MP Biomedicals) was administered in the drinking water for 7 consecutive days. Mice were sacrificed at week 16-post AOM-DSS treatment and colon tissues were removed.

Colons were flushed and fixed overnight in neutral buffered formalin (10%) before paraffin embedding. Briefly, 4µm thick sections were dewaxed in xylene and rehydrated in graded alcohol baths. Slides were incubated in 3% H_2O_2 for 20 min and washed in PBS to quench endogenous peroxidase activity. Antigen retrieval was performed by boiling slides for 20 min in 10 mM sodium citrate buffer, pH 6.0. Nonspecific binding sites were blocked in blocking buffer (TBS, pH 7.4, 5% dried milk, 0.5% Triton X-100) for 60 min at RT. Sections were incubated with anti- β-catenin antibody diluted in blocking buffer overnight at 4°C. Envision+ (Dako) was used as a secondary reagent. Signals were developed with DAB (Sigma-Aldrich). After dehydration, sections were mounted in Pertex (Histolab) and imaged using the Nanozoomer-XR Digital slide Scanner C12000-01 (Hamamatsu).

DNA replication assay, EdU labelling

Cells were treated with 10 µM 5-ethynyl-2'-deoxyuridine (EdU; LifeTechnologies) for the indicated time, harvested, washed once with cold PBS, resuspended in 300µL cold PBS and fixed with 700µL ice-cold 100% ethanol. Click reaction was performed according to the

manufacturer instructions (Click-iT™ Plus EdU Alexa Fluor™ 647 Flow Cytometry Assay Kit; Invitrogen) and cells were analysed by flow-cytometry (BD FACSCanto II). FlowJo® software was used for analysis.

Mammosphere assay

The mammosphere formation assay was performed as previously described[38]. Briefly, 500 cells were plated per well in a low-adherence 96-well plate coated with poly-2-hydroxyethyl-methacrylate (poly-Hema). After 7 days in culture (37°C, 5% CO_2), images of formed mammospheres were acquired and counted using automated high-content microscopy analysis (Cellomics, Thermo).

Aldehyde Dehydrogenase 1 (ALDH1) activity

ALDH1 enzymatic activity was determined using the ALDEFLUOR kit (Stem Cell Technologies) according to the manufacturer instructions. For each sample, half the cell/substrate mixture was treated with diethylaminobenzaldehyde (DEAB; ALDH inhibitor). ALDEFLUOR/DEAB treated cells were used to define negative gates. FACS was performed with $\geq 10^5$ cells.

Xenografts

Animals were housed in the animal facility of IGMM and were maintained in a pathogen-free environment and fed *ad libitum*.

To generate primary tumours, 10^6 cells (4T1) or $3x10^6$ cells (MDA-MB-231) of log-phase viable 'mouse pathogen-free' (Test: IMPACT1, Iddex) were implanted into the fourth inguinal mammary gland (in 50 µl PBS (4T1) or 200 µl PBS (MDA-MB-231)).

Primary tumour volume was measured every week by electronic calliper using the formula "π**/6*S²** (Smaller radius)***L** (Larger radius)".

At the end of the experiment, following sacrifice, primary tumours were excised and fixed over-night in neutral buffered formalin (10%) before paraffin embedding (see above). IHC analysis of Ki-67 expression of the different tumour tissue sections was conducted as described above.

Visualisation of lung metastases

Dissected lungs were stained with 15% India Ink diluted in distilled water, and subsequently washed with 5 ml Fekete's solution (40 ml glacial acid acetic, 80 ml formalin, 580 ml ethanol 100%, 200 ml water). A binocular microscope connected to a digital camera was used to visualise and count the metastatic nodules.

Automated drug library screen

We performed an initial screen of all 1,280 FDA-approved drugs in the Prestwick Chemical Library (Prestwick Chemical, Illkirch-Graffenstaden, France) at 10 µM in white clear-bottom 96-well plates. Briefly, we prepared seeding solutions at a density of 2×10^5 cells/mL in DMEM complete medium (10%FBS), and dispensed 100 µL into 96-well plates using a Multidrop Combi Dispenser (Thermo Scientific™). Next, we prepared 1x treatment solutions of the Prestwick compounds in DMEM complete medium at a concentration of 10 µM using a Tecan EVO200 robotic liquid handling system (Tecan Trading AG). We removed medium from the pre-seeded 96-well plates and we dispensed 100 µL of 1x treatment solutions using the Tecan robot. We incubated plates at 37°C, 5% CO_2 for 48 h in an automated incubator (Cytomat, Thermo Scientific™) associated with the Tecan robot. After treatment, cell survival was determined using the CellTiter-Glo® Luminescent Cell Viability Assay (Promega Corporation) in accordance with the manufacturer's instructions. Luminescence signal was automatically measured with a Tecan Infinity F500 microplate reader (Tecan Trading AG). "Hits" were identified applying the Z-score statistical method (see statistical analysis section). The same method was used for subsequent dose-response experiments on selected "hits".

Induction of anemia with PHZ

Anemia was induced in adult *Mki67*$^{2nt\Delta/2nt\Delta}$ mice and littermate controls (*Mki67*$^{+/2nt\Delta}$) by injection of 40 mg/kg phenylhydrazine (PHZ) on days 0, 1, and 3. Animals were sacrificed on day 5 and blood, spleen and bone marrow were collected. Hematocrit was measured as previously described[39]. Cell suspensions were generated and immunophenotyping performed by flow cytometry.

Immunophenotyping and flow cytometry analyses

Cells isolated from peripheral lymph nodes tumor (draining and non-draining for tumor-bearing mice) as well as spleen and bone marrow, were stained with Sytox blue or Live/dead

fixable viability dye (Life Technologies and eBioscience, respectively) together with the appropriate conjugated anti-CD3, CD45, CD62L, CD4, CD8, CD44, CD25, F4/80, CD19, B220, NK1.1, Gr1, CD11b, CD11c, Ter119, CD71 and Foxp3 antibodies (eBioscience/ThermoFisher or Becton Dickinson, San Diego, CA). Intracellular staining for Foxp3 was performed using the eBioscience Fixation/Permeabilization kit.
Cells were analysed on a FACS Fortessa (BD Biosciences) flow cytometer. Data analyses were performed using FlowJo Mac v.10 (Tree Star) or DIVA (Becton Dickinson) software.

Prior to intracellular cytokine stainings, cells were activated with PMA (Sigma-Aldrich; 100 ng/ml)/ Ionomycin (Sigma-Aldrich; 1ug/ml) in the presence of brefeldin A (Sigma-Aldrich; 10ug/ml) for 3.5-4h at 37°C. Cell surface staining was performed, after which cells were fixed and permeabilised using a fixation/permeabilization kit (BD Biosciences or eBioscience) followed by intracellular cytokine staining.

Antibodies used for immunophenotying

	clone	fluorochrome	reference
Murine anti-CD3	145-2C11	V421	562600
Murine anti-CD4	RM4-5	BV711	563726
Murine anti-CD8	53-6.7	FITC	553031
Murine anti-CD8	53-6.7	AF700	564983
Murine anti-CD62L	MEL-14	APC	553152
Murine anti-CD44	IM7	PE-CF594	562464
Murine anti-CD45	30-F11	AAF	47-0451-82
Murine anti-CD25	PC61	AAF	47-0251-82
Murine anti-CD19	1D3	BV650	563235
Murine anti-NK11	PK136	APC	550627
Murine anti-CD11b	M1/70	BV605	563015
Murine anti-CD11c	HL3	PE	557401
Murine anti-LY6G	RB6-8C5	PE-CF594	562710
Murine anti-LY6C	AL-21	V450	560594
Murine anti-F4/80	BM8	PEC7	25-4801-82
Murine anti-Foxp3	FJK-16S	PEC7	25-5773-82
Murine anti-TNFα	MP6-XT22	PE	12-7321-82
Murine anti-IL-2	JES6-5H4	PEC7	560538
Murine anti-IFNγ	XMG1.2	APC	17-7311-82
Murine anti-IL17A	TC11-18H10	BV605	564169
Murine anti-Ter119	Ter-119 (hamster)	FITC	557915

Murine anti-CD71	C2	BV605	563013
Murine anti-B220	RA3-6B2	eF780	47-0452-82

149

150 **Cell extracts and Western-blotting**

151 Frozen cell pellets (harvested by trypsinization, washed with cold PBS) were lysed directly
152 in Laemmli buffer at 95°C. Protein concentrations were determined by BCA protein assay
153 (Pierce Biotechnology). Proteins were separated by SDS-polyacrylamide gel
154 electrophoresis (SDS-PAGE) (7.5% and 12.5% gels) and transferred to Immobilon
155 membranes (Milipore) at 1.15 mA/cm^2 for 120 min with a semi-dry blotting apparatus.
156 Membranes were blocked in TBS-T pH 7.6 (20 mM Tris, 140mM NaCl, 0.1% Tween-20)
157 containing non-fat dry milk (5%), incubated with the primary antibody for 2 hours at RT or
158 over-night at 4°C, washed several times with TBS-T for a total of 45 minutes, incubated with
159 secondary antibody at 1/5000 dilution for 1 hour at RT and washed several times in TBS-T.
160 Signals were detected using Western Lightning Plus-ECL (PerkinElmer) and Amersham
161 Hyperfilm^{TM} (GE Healthcare).

162

163 **qRT-PCR**

164 For reverse transcription (cDNA synthesis), 500 ng of purified RNA in total volume of 10µl,
165 extracted by RNeasy Mini Kit (Qiagen), were mixed with 1µl of 10mM dNTPs mix
166 (LifeTechnologies) and 1µl of 50µM random hexaprimers (NEB). Samples were incubated
167 at 65°C for 5 minutes, transferred to ice, 5µl 5x First Strand Buffer, 2µLl100mM DTT and 1µl
168 RNasin RNase Inhibitor (Promega) were added and samples were incubated at 25°C for 10
169 minutes, 42°C for 2 minutes. 1µl of SuperScript® III Reverse Transcriptase
170 (LifeTechnologies) was added to each sample and incubated at 50°C for 60 minutes, 70°C
171 for 15 minutes.
172 qPCR was performed using LightCycler® 480 SYBR Green I Master (Roche) and
173 LightCycler® 480 qPCR machine. The reaction contained 5ng of cDNA, 2µl of 1µM qPCR
174 primer pair, 5µl 2x Master Mix, and final volume made up to 10µl with DNase free water.
175 Primers used for both mouse (Mki67) and human (MKI67) Ki-67 in addition to the
176 housekeeping genes are similar to those used by Sobecki et al., 2016. qPCR was conducted
177 at 95°C for 10 min, and then 40 cycles of 95°C 20s, 58°C 20s and 72°C 20s. The specificity
178 of the reaction was verified by melting curve analysis.

179

180 **PCR primers used in this study.**

181

Gene name	Sequence	PrimerBank ID	Reference
Actb	Fw- GGCCCAGAGCAAGAGAGGTATCC Rv- ACGCACGATTTCCCTCTCAGC	-	[40]
Gapdh	Fw- CGTCCCGTAGACAAAATGGT Rv- TGACTGTGCCGTTGAATTTG	-	[41]
B2m	Fw- ACGTAACACAGTTCCACCCG Rv- CAGTCTCAGTGGGGGTGAAT	-	[42]
Gusb	Fw- AACAACACACTGACCCCTCA Rv- ACCACAGATCGATGCAGTCC	-	[42]
Zeb2	Fw- GGCAAGGCCTTCAAGTACAA Rv- AAGCGTTTCTTGCAGTTTGG	-	[43]
Twist1	Fw- AGCGGGTCATGGCTAACG Rv- GGACCTGGTACAGGAAGTCGA	-	[44]
Tap2	Fw- CTGGCGGACATGGCTTTACTT Rv- CTCCCACTTTTAGCAGTCCCC	7549791a1	[45]
Psmb8	Fw- ATGGCGTTACTGGATCTGTGC Rv- CGCGGAGAAACTGTAGTGTCC	6755208a1	[45]
Zeb1	Fw- CGCCATGAGAAGAACGAGGAC Rv- CTGTGAATCCGTAAGTGCTCTTT	357197186c2	[45]
Vim	Fw- CTGCTTCAAGACTCGGTGGAC Rv- ATCTCCTCCTCGTACAGGTCG	227430362c2	[45]
Epcam	Fw- GGAGTCCCTGTTCCATTCTTCT Rv- GCGATGACTGCTAATGACACCA	11229327c3	[45]
Hes1	Fw- GATAGCTCCCGGCATTCCAAG Rv- GCGCGGTATTTCCCCAACA	31560817c2	[45]
Lef1	Fw- GCCACCGATGAGATGATCCC Rv- TTGATGTCGGCTAAGTCGCC	118130133c1	[45]
Aldh1l2	Fw- TTTCCTGAGGGGATCAAGGC Rv- GACCTCGAATCCAGTTATGCAA	283436217c3	[45]
Aldh3a1	Fw-AATATCAGTAGCATCGTGAACCG Rv- GGAGAGCCCCTTAATCGTGAAA	6680676a1	[45]

Colony formation assay

3T3 wild-type (WT) and two Ki-67 TALEN-mutant clones were transduced with either empty control or H-Ras^{G12V} expressing retroviruses. After verification of Ras^{G12V} expression, cells were seeded at 10^5 cells/well (6 well-plate) in triplicate and allowed to grow for 2-weeks

(media were changed every 2 days). Cells were then fixed (4% formaldehyde) and stained with 0.5% (w/v) crystal violet to visualise the colonies formed.

RNA sequencing library prep

Total RNA was extracted using Trizol (Life Technologies) following manufacturer's instructions from wild type and two clones of 4T1 Ki-67 knockout cell lines. RNA integrity was analysed on Agilent 2100 bioanalyzer. For library preparation, cDNA synthesis was performed on rRNA-depleted samples using the TruSeq Stranded Total RNA Library Preparation (RS-122-2301). All sequencing libraries were prepared in two or three biological replicates. Indexed cDNA libraries were sequenced by MGX (Montpellier) on Illumina HiSeq2000 with a single 50 bp read and a 10 bp index read.

Sequencing of cDNA libraries and data processing

FastQC was used to perform quality control of the sequencing. Using the tool STAR 2.6.0a(2), all the reads that passed the quality control were aligned to the mouse reference genome (GRCm38.p6) and the counts per gene were quantified. The release 93 of the Ensembl mouse genome annotations were used for establishing the coordinates of each gene and their transcripts. Differential expression analysis was performed in R using the DESeq2(2) library embedded in an in-house script. After normalization of the read counts per gene, a negative binomial generalised linear model was fitted considering single factor design for assessing the differential expression between Mki67 knockout and wild-type samples. Gene set enrichment analysis of the 4T1 *Mki67*$^{-/-}$ cell line vs WT cell line was performed using the javaGSEA(3) desktop application with a log-fold-change pre-ranked gene list.

Gene set enrichment for transcription factors.

The gene set enrichment was performed over the ENCODE and ChEA Consensus TFs from ChIP-X gene set, which contains consensus target genes for transcriptions factors present in ENCODE and ChEA databases. The p value was computed with the Fisher Exact test and then adjusted for multiple hypotesis testing in order to obtain the FDR (false discovery rate) adjusted p-value.

MHC class I expression analysis

The MHC class I expression analysis was performed as previously described[46]. 4T1 CTRL and *Mki67*$^{-/-}$ cells were incubated with anti-H2D^{d}-FITC, anti-H2K^{d}-PE or control isotypes, and

MDA-MB-231 CTRL and *Mki67*$^{-/-}$ cells were incubated with anti-HLA-PE or control isotype, in PBS/BSA 2% at 4°C for 20 min. After 2 washes in PBS/BSA 2%, cells were analysed by FACS.

Statistical analysis

Significant differences between the different experimental groups were tested using an unpaired two-tailed Student's *t*-test or ANOVA in Prism 5 (GraphPad). For all analyses, p values < 0,05 (*), p values < 0,01 (**), p values < 0,001 (***) and p values < 0,0001 (****) were considered to indicate a statistically significant result.

37. Shalem, O. *et al.* Genome-scale CRISPR-Cas9 knockout screening in human cells. *Science* **343**, 84–7 (2014).
38. Shaw, F. L. *et al.* A detailed mammosphere assay protocol for the quantification of breast stem cell activity. *J. Mammary Gland Biol. Neoplasia* **17**, 111–117 (2012).
39. Oburoglu, L. *et al.* Glucose and glutamine metabolism regulate human hematopoietic stem cell lineage specification. *Cell Stem Cell* **15**, 169–184 (2014).
40. Leeb, M. *et al.* Polycomb complexes act redundantly to repress genomic repeats and genes. *Genes Dev.* **24**, 265–276 (2010).
41. Sanli, I. *et al.* Meg3 Non-coding RNA Expression Controls Imprinting by Preventing Transcriptional Upregulation in cis. *Cell Rep.* **23**, 337–348 (2018).
42. Panina, Y., Germond, A., Masui, S. & Watanabe, T. M. Validation of Common Housekeeping Genes as Reference for qPCR Gene Expression Analysis During iPS Reprogramming Process. *Sci. Rep.* **8**, 8716 (2018).
43. Lin, Y. *et al.* Snail1-dependent control of embryonic stem cell pluripotency and lineage commitment. *Nat. Commun.* **5**, 3070 (2014).
44. Hahn, S. *et al.* Organoid-based epithelial to mesenchymal transition (OEMT) model: from an intestinal fibrosis perspective. *Sci. Rep.* **7**, 2435 (2017).
45. Spandidos, A., Wang, X., Wang, H. & Seed, B. PrimerBank: a resource of human and mouse PCR primer pairs for gene expression detection and quantification. *Nucleic Acids Res.* **38**, D792-799 (2010).
46. Charni, S. *et al.* Oxidative phosphorylation induces de novo expression of the MHC class I in tumor cells through the ERK5 pathway. *J. Immunol. Baltim. Md 1950* **185**, 3498–3503 (2010)